ACS APPLIED MATERIALS & INTERFACES

Research Article

www.acsami.org

Tailored Electronic Structure and Optical Properties of Conjugated Systems through Aggregates and Dipole−Dipole Interactions

Young Il Park,[†] Cheng-Yu Kuo,[†] Jennifer S. Martinez,[‡] Young-Shin Park,[†] Olena Postupna,[§] Andriy Zhugayevych,[§] Seungho Kim,[∥] Jongwook Park,[∥] Sergei Tretiak,*[,§] and Hsing-Lin Wang*[,†]

[†]C-PCS, Chemistry Division, [‡]Center of Integrated Nanotechnologies, Materials Physics and Application Division, and [§]Theory Division, Los Alamos National Laboratory, Los Alamos, New Mexico, 87545, United States

[∥]Department of Chemistry/Display Research Center, The Catholic University of Korea, Bucheon 420-743, Republic of Korea

Supporting Information

ABSTRACT: A series of PPVO (*p*-phenylene vinylene oligomer) derivatives with functional groups of varying electronegativity were synthesized via the Horner−Wadsworth−Emmons reaction. Subtle changes in the end group functionality significantly impact the molecular electronic and optical properties of the PPVOs, resulting in broadly tunable and efficient UV absorption and photoluminescence spectra. Of particular interest is the NO_2-substituted PPVO which exhibits photoluminescence color ranging from the blue to the red, thus encompassing the entire visible spectrum. Our experimental study and electronic structure calculations suggest that the formation of aggregates and strong dipole−dipole solute−solvent interactions are responsible for the observed strong solvatochromism. Experimental and theoretical results for the NH_2-, H-, and NO_2-substituted PPVOs suggest that the stabilization of ground or excited state dipoles leads to the blue or red shift of the optical spectra. The electroluminescence (EL) spectra of H-, COOH-, and NO_2-PPVO have maxima at 487, 518, and 587 nm, respectively, in the OLED device. This trend in the EL spectra is in excellent agreement with the end group-dependent PL spectra of the PPVO thin-films.

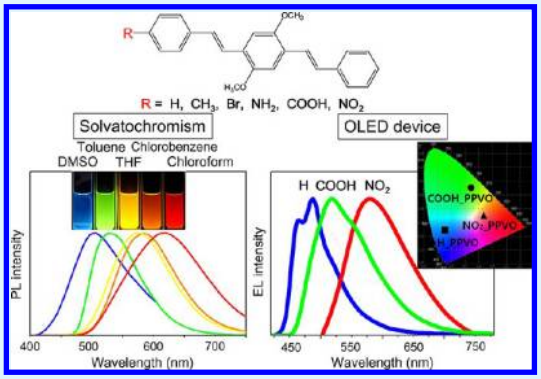

KEYWORDS: *phenylene vinylene, Horner−Wadsworth−Emmons reaction, solvatochromism, aggregates, dipole−dipole interactions, OLED*

INTRODUCTION

Conjugated polymers/oligomers have received worldwide attention because of their applications in optoelectronics, light emitting diodes (LED)[1,2] and organic photovoltaic devices.[3−6] Conjugated oligomers constitute a unique class of materials possessing the optical and electronic properties of the conjugated polymers, while still having a well-defined structure allowing complete characterization and determination of structure−properties relationships.[7,8] Therefore, predictive design and synthesis of conjugated polymers/oligomers, with energetics that meet the requirements of optoelectronic devices, is an area of intense research effort. Of particular interest are the *p*-phenylene vinylene oligomer (PPVO) derivatives, one of the most extensively studied conjugated oligomers owing to their high quantum yield and tunable structures that lead to desired physical and electronic properties.[9−11] Beyond chemical derivatization, the properties of PPVO can be further modulated by the interaction with solvent and formation of aggregates, which represent two major avenues for achieving control over structural homogeneity and optical properties in solutions and thin films.[7,12,13] Unlike conjugated polymers, PPVOs can have distinctive ground state and excited state dipoles that can be preferentially stabilized by the solvent. Thus, we can fine-tune the electronic structure of the conjugated oligomers by either varying the conjugation length of the molecule or by attaching substituents and functional groups with different electron affinities.[14−16] Many studies have explored design of oligomers with donor−acceptor characteristics embedded within the structure[17,18] to confer intramolecular charge transfer properties and expand the absorption into the low energy region.[19−21] Such strategies have been widely adopted to synthesize low band gap molecules for fabricating photovoltaic and electrochromic devices.[18,22] Tailoring synthesis to modulate absorption and emission characteristics of conjugated oligomers has been extensively studied for the past decade to improve the material performance and device efficiency.[23] Despite all the studies above, there is limited understanding of the chemical and physical principles that determine the dipole interactions and aggregate formation, which prevents predictive design of PPVO with desired optical and electronic properties.

Received: December 5, 2012
Accepted: April 22, 2013
Published: April 22, 2013

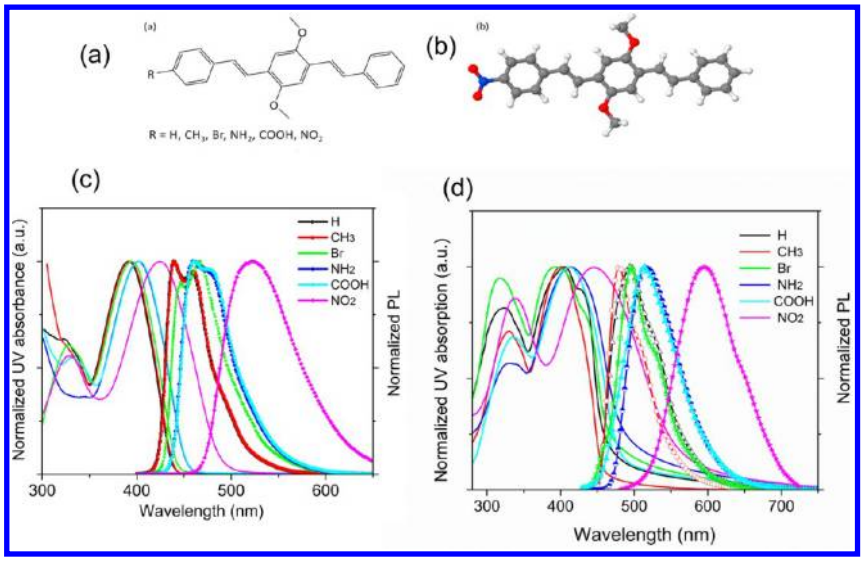

Figure 1. (a) Chemical structure of the functionalized PPVO and (b) ground state geometry of the NO_2-terminated molecule. The normalized UV–vis spectra (line) and PL spectra (line+symbol) (c) in solution with concentration of 1×10^{-4} M (d) thin films cast from toluene solutions.

Scheme 1. Synthetic Scheme of PPVO Derivatives

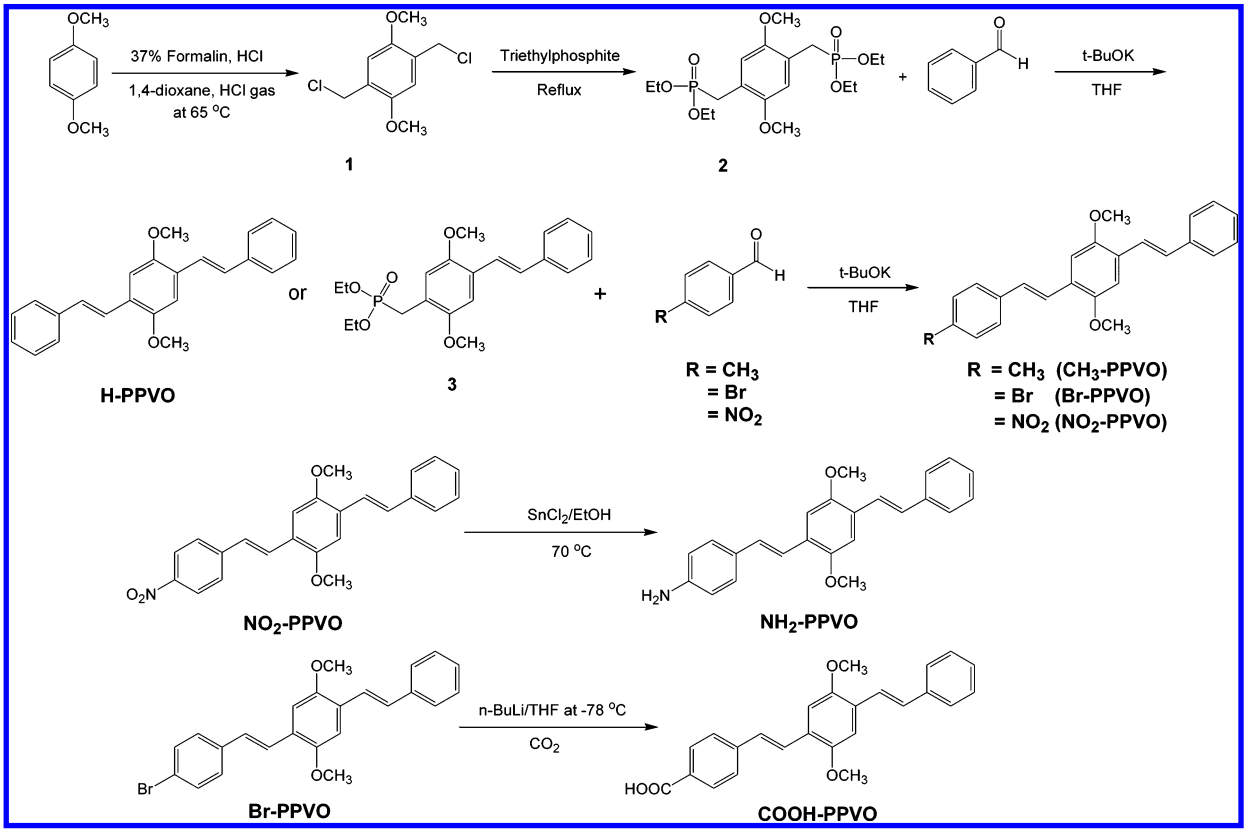

In this manuscript, we have demonstrated the synthesis and characterization of a family of ((1*E*,1′*E*)-(2,5-dimethoxy-1,4-phenylene)bis(ethene-2,1-diyl))dibenzene derivatives: a series of PPVO with two methoxy substituents at the 2 and 5 positions of the central benzene ring. These PPVOs differ only by the end group functionality (see Figure 1a, b) yet exhibit strong end-group-dependent physical and optical properties. Systematic variation of oligomer end groups allows us to assess the impact that dipole interactions and aggregate formation have on the electronic and optical properties of conjugated systems. Our study offers valuable insights into how subtle changes in molecular structure of oligomers and processing methods result in tailored electronic structure and optical properties for highly efficient molecular, electronic, and photovoltaic devices.

EXPERIMENTAL SECTION

Synthesis. The synthetic scheme for the six PPVO derivatives, terminated by functional groups of varying electronegativity, via Horner–Wadsworth–Emmons reaction is shown in Scheme 1. Synthesis is achieved via reacting phosphonate carbanions with

dx.doi.org/10.1021/am400766w | ACS Appl. Mater. Interfaces 2013, 5, 4685–4695

aldehydes (or ketones) to produce predominantly *E*-alkenes. All reagents and solvents were purchased from Aldrich or Fisher and were used without further purification.

*Synthesis of 1,4-Bis-chloromethyl-2,5-dimethoxy-benzene (**1**).* 1,4-Dimethoxy-benzene (10 g, 0.07 mol), concentrated HCl (10 mL) and 37% formalin solution in H_2O (15 mL) were added in 1,4-dioxane (50 mL). The reaction mixture was heated to 65 °C for 6 h. The white solution was cooled and filtered. The solid was washed with acetone and dried. A white product was obtained (14.4 g, yield = 85%). ^{1}H NMR (400 MHz, $CDCl_3$): δ 3.86 (s, 6H), 4.65 (s, 4H), 6.93 (s, 2H).

*Synthesis of [4-(Diethoxy-phosphorylmethyl)-2, 5-dimethoxy-benzyl]-phosphonic Acid Diethyl Ester (**2**).* Compound **1** (10 g, 42.5 mmol) and triethylphosphite (21.1 mL, 127.5 mmol) were added and purged with nitrogen gas. The reaction mixture was refluxed for 24 h. The solution was cooled, and the residue was extracted with chloroform. The solution was dried over $MgSO_4$, filtered, and stripped of the solvent by rotary evaporation. Recrystallization of the residue from chloroform and hexane afforded a white product (18.6 g, yield = 100%). ^{1}H NMR (400 MHz, $CDCl_3$): δ 1.25 (m, 12H), 3.23 (d, 4H), 3.79 (s, 6H), 4.03 (m, 8H), 6.90 (s, 2H).

*Synthesis of (2, 5-Dimethoxy-4-styryl-benzyl)-phosphonic Acid Diethyl Ester (**3**).* Compound **2** (10 g, 22.8 mmol) and benzaldehyde (0.8 g, 7.6 mmol) were added and purged with nitrogen gas. Anhydrous THF (100 mL) was added to the flask and followed by the addition of 45 mL of 1 M t-BuOK in THF via addition funnel. The mixture was allowed to stir at room temperature for 4 h and poured into 6 M HCl (20 mL) to afford a yellow solution. The solution was extracted with chloroform and dried over $MgSO_4$, further filtered, and stripped of the solvent by rotary evaporation. The residue was purified on a silica gel column using ethyl acetate to afford a yellow liquid (6.6 g, yield 75%). ^{1}H NMR (400 MHz, $CDCl_3$): δ 1.26 (m, 6H), 3.28 (d, 2H), 3.84 (s, 6H), 4.08 (m, 4H), 6.94–7.34 (m, 9H).

Synthesis of 1,4-Dimethoxy-2,5-distyryl-benzene (H-PPVO). Yellow solid. ^{1}H NMR (400 MHz, DMSO-d_6): δ 3.90 (m, 6H), 7.24–7.28 (m, 2H), 7.31–7.45 (m, 10H), 7.56–7.58 (d, 4H). ^{13}C NMR (400 MHz, $CDCl_3$): δ (ppm) 56.6, 109.4, 123.4, 123.4, 126.8, 127.7, 128.8, 129.2, 138.0, 151.7. FT-IR (KBr, cm^{-1}): 3040, 2991, 2931, 2856, 2826, 1592, 1489, 1459, 1405, 1343, 1330, 1258, 1212, 1177, 1046, 959, 842, 757, 748, 693, 599, 507. Mass spectrum EI calcd m/z of [M] = 342.16, measured m/z of [M] = 342.07.

General Horner–Emmons Reaction (CH_3-PPVO, Br-PPVO, NO_2-PPVO). Compound **3** (1 mmol) and an aromatic aldehyde derivative (1 mmol) was added and purged with nitrogen gas. Anhydrous THF (10 mL) was added to the flask and followed by the addition of 2.5 mL of 1 M t-BuOK in THF via addition funnel. The mixture was allowed to stir at room temperature for 4 h and poured into 6 M HCl (20 mL) to afford a yellow solution. The solution was extracted with chloroform and dried over $MgSO_4$, and further filtered, and stripped of the solvent by rotary evaporation. The residue was purified on a silica gel column using ethyl acetate/hexane. CH_3-, Br-, and NO_2-PPVOs were obtained and were organic spectroscopy data are listed in the following sections.

1,4-Dimethoxy-2-styryl-5-(2-p-tolyl-vinyl)-benzene (CH_3-PPVO). Yellow solid (yield 88%). ^{1}H NMR (400 MHz, DMSO-d_6): δ 2.30 (s, 3H), 3.89 (s, 6H), 7.18–7.19 (d, 2H), 7.26–7.35 (m, 6H), 7.37–7.47 (m, 5H), 7.56–7.58 (d, 2H). ^{13}C NMR (400 MHz, $CDCl_3$): δ (ppm) 21.4, 56.6, 109.3, 109.4, 115.7, 122.4, 123.5, 126.6, 126.7, 127.0, 127.6, 128.8, 129.0, 129.1, 129.5, 135.2, 137.5, 138.0, 151.6. 151.7. FT-IR (KBr, cm^{-1}): 3040, 2992, 2927, 2859, 2829, 1513, 1491, 1458, 1449, 1407, 1340, 1332, 1258, 1204, 1178, 1043, 962, 846, 803, 750, 704, 687, 506. Mass spectrum EI calcd m/z of [M] = 356.18, measured m/z of [M] = 356.10.

1-[2-(4-Bromo-phenyl)-vinyl]-2,5-dimethoxy-4-styryl-benzene (Br-PPVO). Yellow solid (yield 84%). ^{1}H NMR (400 MHz, DMSO-d_6): δ 3.89 (s, 6H), 7.33–7.42 (m, 9H), 7.53–7.58 (m, 6H). ^{13}C NMR (400 MHz, $CDCl_3$): δ (ppm) 56.6, 105.2, 109.3, 123.4, 124.2, 126.8, 127.7, 127.8, 128.2, 128.8, 129.4, 131.9, 137.0, 138.0, 151.7. FT-IR (KBr, cm^{-1}): 3040, 2991, 2931, 2831, 1506, 1496, 1484, 1458, 1448, 1408, 1340, 1331, 1257, 1207, 1179, 1071, 1043, 1005, 962, 853, 808, 751, 687, 667, 507. Mass spectrum EI calcd m/z of [M] = 420.07, measured m/z of [M] = 420.02.

1,4-Dimethoxy-2-[2-(4-nitro-phenyl)-vinyl]-5-styryl-benzene (NO_2-PPVO). Orange solid (yield 86%). ^{1}H NMR (400 MHz, DMSO-d_6): δ 3.92 (d, 6H), 7.27–7.29 (t, 1H), 7.37–7.59 (m, 10H), 7.64–7.68 (d, 2H), 7.82–7.84 (d, 2H). ^{13}C NMR (400 MHz, $CDCl_3$): δ (ppm) 56.6, 109.3, 109.7, 123.2, 124.3, 125.4, 126.6, 126.9, 127.0, 127.9, 128.2, 128.9, 130.0, 144.8, 152.3. FT-IR (KBr, cm^{-1}): 3036, 2998, 2941, 2831, 1624, 1585, 1558, 1509, 1463, 1410, 1334, 1319, 1291, 1261, 1211, 1178, 1108, 1042, 959, 871, 830, 856, 752, 696. Mass spectrum EI calcd m/z of [M] = 387.15, measured m/z of [M] = 387.62.

Synthesis of 4-[2-(2,5-Dimethoxy-4-styryl-phenyl)-vinyl]-phenyl-amine (NH_2-PPVO). NO_2-PPVO (0.5 g, 1.29 mmol) was purged with nitrogen gas. 40% Stannous chloride (1.34 mL) was added to the flask and allowed to stir at 70 °C for 18 h. Once the reaction was complete, 5% $NaHCO_3$ solution was added slowly to a final pH of 8. The solution was extracted with ethyl acetate. The solution was dried over $MgSO_4$, filtered, and stripped of the solvent by rotary evaporation. The residue was purified on a silica gel column using ethyl acetate/hexance (1:1) to afford a orange solid (0.34 g, yield 70%). ^{1}H NMR (400 MHz, DMSO-d_6): δ 3.87 (d, 6H), 5.31 (s, 2H), 6.55–6.57 (d, 2H), 7.10–7.12 (d, 2H), 7.23–7.30 (m, 5H), 7.35–7.38 (m, 4H), 7.55–7.56 (d, 2H). ^{13}C NMR (400 MHz, $CDCl_3$): δ (ppm) 56.6, 109.0, 109.4, 115.3, 119.7, 123.5, 126.7, 127.5, 128.0, 128.7, 129.2, 146.2, 151.4, 151.8. FT-IR (KBr, cm^{-1}): 3456, 3356, 3043, 2988, 2938, 2831, 1616, 1606, 1589, 1575, 1558, 1515, 1507, 1495, 1465, 1457, 1410, 1342, 1278, 1260, 1212, 1184, 1176, 1043, 958, 845, 819, 805, 752, 689, 668, 572, 520, 508. Mass spectrum EI calcd m/z of [M + H$^+$] = 357.17, measured m/z of [M + H$^+$] = 358.10.

Synthesis of 4-[2-(2,5-Dimethoxy-4-styryl-phenyl)-vinyl]-benzoic acid (COOH-PPVO). Br-PPVO (0.2 g, 0.47 mmol) were purged with nitrogen gas and cooled to 78 °C. 1.6 M *n*-BuLi (0.38 mL) was added to the flask and kept at −78 °C for 1 h. Excess dry ice (at least 0.5 g) was added. After the reaction was complete, 1.5 M H_2SO_4 was added to acidify the solution. The solution was extracted with ethyl acetate. The solution was dried over $MgSO_4$, filtered, and stripped of the solvent by rotary evaporation. The residue was purified on a silica gel column using ethyl acetate/hexane (1:3) to afford a yellow solid (0.20 g, yield 72%). ^{1}H NMR (400 MHz, DMSO-d_6): δ 3.90 (d, 6H), 7.25–7.26 (t, 1H), 7.28–7.45 (m, 7H), 7.53–7.59 (m, 3H), 7.66–7.68 (d, 2H), 7.92–7.94 (d, 2H), 12.95 (s, 1H). ^{13}C NMR (400 MHz, $CDCl_3$): δ (ppm) 56.6, 109.4, 109.6, 123.3, 126.0, 126.6, 126.8, 127.8, 128.8, 129.7, 130.8, 137.9, 143.5, 151.7, 152.1, 171.1. FT-IR (KBr, cm^{-1}): 3049, 3003, 2953, 2863, 2830, 2666, 2541, 1683, 1601, 1489, 1465, 1411, 1345, 1315, 1291, 1260, 1208, 1179, 1044, 964, 851, 770, 755, 696, 553, 507. Mass spectrum EI calcd m/z of [M] = 386.15, measured m/z of [M] = 386.08.

Characterization. All reagents and solvents are purchased from Aldrich or Fisher and used without further purification. ^{1}H and ^{13}C NMR spectra were recorded on a Bruker Avance 400 spectrometer. The IR spectra were recorded on a NICOLET-750 FT-IR spectrometer with KBr. Mass spectra were recorded on a Waters Synapt G2-S. The optical absorption and fluorescence spectra were obtained with Varian Cary 500 and Varian Cary Eclipse spectrometers. Quantum yields (QY) of PPVO solutions were measured using toluene as solvent and diphenylanthracene as standard, (see Supporting Information Figure S3). PL spectra of the PPVO solutions were obtained using excitation wavelength at ∼370 nm. Cyclic voltammetry was performed at a concentration of 0.1 M for synthesized materials dissolved in acetonitrile with tetrabutylammonium perchlorate (TBAP) as an electrolyte. The working and counter electrodes were Pt against an $Ag/AgNO_3$ reference electrode. Cyclic voltammograms were acquired at a scan rate of 100 mV/s. Ferrocene was used for potential calibration. Band gap energy was estimated by the intersect of extrapolating tangent lines at the red edge of the absorption peak. The LUMO energies of the PPVOs were obtained by adding HOMO energy and the band gap energy. OLED devices were fabricated using the PPVOs as the emitting layer in the following structure: ITO/NPB (30 nm)/TCTA (20 nm)/PPVO derivatives (30

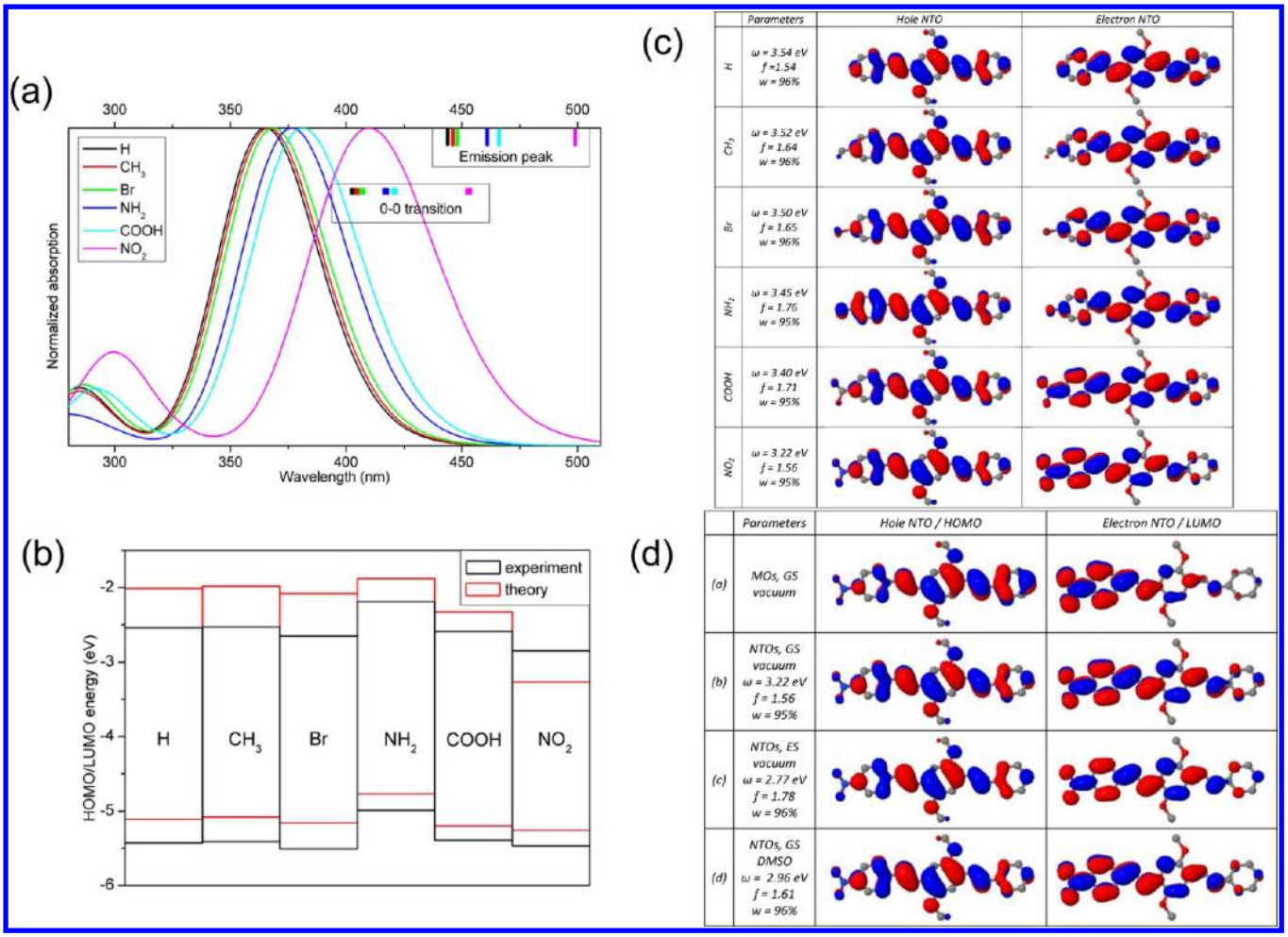

Figure 2. (a) Calculated absorption spectra, emission peak positions, and 0−0 transition energies for different functional groups in toluene. (b) Calculated vs experimentally determined HOMO/LUMO levels (i.e., IP/EA) in acetonitrile. (c) NTOs for the first transition in vacuum in the ground state geometry: dependence on the functional group; here ω is the transition energy, f is the oscillator strength, and w is the weight of the given NTO pair in the corresponding transition density matrix. (d) Comparison of NTOs for the first transition under different conditions and frontier MOs for NO_2 group: (a, b) MO vs NTO, (b, c) ground (GS) vs excited state (ES) geometry, and (b, d) in vacuum vs in DMSO.

nm)/TPBi (30 nm)/LiF (1 nm)/Al, where NPB was used for the hole injection layer (HIL), TCTA was the hole transport layer (HTL) and exciton blocking layer (EBL), and TPBi was the electron transport layer (ETL). All organic layers were deposited under 10^{-6} Torr, with a rate of deposition of 1 Å/s to give an emitting area of 4 mm^2. The light intensity of EL device was obtained with a Minolta CS-1000A and a Keithley 2400 electrometer.

Electronic Structure Modeling. Quantum-chemical calculations have been performed on a series of functionalized PPVO (Figure 1a) in a wide range of organic solvents. Calculations of ground state properties have been done using density functional theory (DFT). Modeling of excited states have been done using time-dependent DFT (TDDFT), providing a method of choice for modeling optical spectra in a broad variety of medium-sized molecular systems. All calculations are conducted using the CAM-B3LYP functional combined with the 6-31G basis set as implemented in the Gaussian09 program package.[24] CAM-B3LYP is a long-range corrected hybrid functional resolving multiple issues of the widely used B3LYP parent model with better description of neutral excitations and charged states in extended π-conjugated systems.[25−27] The 6-31G basis set is known to provide adequate results for geometry and energy values for relatively large molecules consisting of the first row elements[28−30] in a noticeably short CPU time. A selected set of calculations (for H- and NO_2-functionalized molecules in vacuum and DMSO) is also modeled using the 6-31G* basis set. Since results obtained with these two sets differ insignificantly, the least resource consuming set has been used for subsequent simulations.

Solvent effects are accounted for using conductor-like polarizable continuum model (CPCM)[31,32] with the appropriate dielectric constants (Supporting Information Table S2). Results of calculations performed with the PCM model (the default solvation model in Gaussian09), are found to differ insignificantly from those obtained with CPCM for all molecules in toluene.

Ground-state molecular geometries have been optimized in vacuum and in all solvents. In all cases, the obtained geometries are topologically equivalent to the one shown in Figure 1b. Electron affinity (EA) and ionization potential (IP) values have been obtained from the energies of the cationic and anionic species at their respective optimal geometries. The lowest excited states are optimized starting from the ground state geometries in a corresponding media. To simulate absorption (emission) spectra, the vertical transition energies and their corresponding oscillator strengths have been calculated using ground (excited) state optimal geometries. Resulting spectral lines are broadened with the Gaussian function to obtain spectral profiles to guide the eye. Finally, the nature of the calculated excited states has been analyzed in terms of natural transition orbital (NTOs) providing a convenient way to identify and visualize electronic excitations.[33]

RESULTS AND DISCUSSIONS

UV−vis Absorption Spectra. The end groups attached to the PPV oligomer have different electronegativities (electron affinity decreases along the following sequence: nitro, amino, bromo, carboxylate, methyl, and unsubtituted oligomers). Consequently, the optical properties of substituted conjugated oligomers show a strong correlation between the absorption/emission spectra and associated molecular dipoles (Figures 1−5, Supporting Information Table S1). Structurally, PPVOs could have cis−cis, cis−trans, and trans−trans configurations whose optical properties are distinctly different from one another.[34] We have determined that all molecules in our study have trans−trans configuration, judging from their FT-IR and NMR spectra (Supporting Information Figure S1). There are two characteristic broad absorption peaks in the UV−vis spectra of all PPVOs manifesting distinct electronic transitions. For example, in toluene (Figure 1c), all six PPVOs have a higher energy absorption band with a λ_{max} at roughly 330 nm. For the low energy absorption peak S_1, λ_{max} varies from 391 nm for H, CH_3, and Br-PPVO to 425 nm for NO_2-PPVO. Similarly, two distinct UV−vis absorption peaks are observed in other solvents such as chloroform (Supporting Information Figure S2a and b). Overall, the UV−vis absorption spectra suggest that PPVO exhibit moderate change in λ_{max} of the S_1 state, for example, in toluene λ_{max} of S_1 varies no more than 37 nm (see Supporting Information Table S1 summarizing λ_{max} position of the S_1 peak in solvents and thin films). The UV−vis spectra of thin films follow similar trends in terms of shifting of λ_{max} as compared to the solution (Figure 1d). Notably, for the same PPVO molecule, the λ_{max} of the thin film absorption spectra are slightly red-shifted (by about 10−20 nm) compared to solution, indicative of less conformational disorder in the solid state due to packing of the PPVO molecules. Moreover, a stronger electronic coupling between PPVO in a film may also contribute to the red-shifts of the optical spectra.

Our electronic structure calculations are able to quantitatively reproduce the overall shape and the relative peak positions of the experimentally obtained absorption spectra (Figure 2a). For the strongest absorption peak, S_1, calculated vertical excitation energies are systematically blue-shifted by 15−25 nm (0.1−0.2 eV, see Figure 3) compared to the experimental λ_{max} position. This difference in the λ_{max} is consistent with the typical accuracy of time-dependent density functional theory (TDDFT) modeling when one neglects vibronic effects.[35] Notably, theoretical results are able to reproduce all relative trends in absorption spectra as a function of the end group substitution (see detailed analysis below). Examination of the natural transition orbitals (NTOs) corresponding to the lowest strongly allowed electronic transition (Figure 2c) reveals that the excited state represents a typical $\pi-\pi^*$ S_0-S_1 transition, where hole and electron NTOs mostly correspond to HOMO and LUMO molecular orbitals, respectively (Figure 2d). While the hole NTO is nearly uniformly distributed over the conjugated backbone, we note that the electron NTO becomes more and more localized toward the end group with an increase of substituent electronegativity. This trend indicates that the lowest excitation gains charge-transfer (CT) character and gradually transitions into a typical intramolecular CT excitation. Notice that for a given molecule, the characteristic form of calculated NTOs does not depend on the presence of solvent and is retained at the excited state optimal geometry relevant to emission (Figure 2d). Finally, our calculations attribute the second high energy absorption peak to a combination of several weakly allowed high energy $\pi-\pi^*$ delocalized transitions.

Dipole−Dipole Interactions and PL Spectra. Compared to the UV−vis absorption spectra, the emission spectra variations with respect to the end group functionality and solvent are much more dramatic. For the most part, these changes are due to strong dipole−dipole interactions between solvent and solute as well as aggregation effects. For example, strong variation of the emission color with respect to the end group functionality is observed for the PL spectra of the toluene solution (Figure 1c). We notice that PL of all substituted PPVO, with the exception of the NO_2−PPVO, exhibit vibronic features (i.e., distinct 0−0 and 0−1 transitions associated with a typical C−C stretching motion strongly coupled to the electronic system) suggesting the dominance of single molecule species. The lack of such vibronic features in the emission spectra for the NO_2-PPVO is indicative of a highly aggregated species in solution. The Stokes shifts for all compounds are strongly related to their structures. The Stokes shifts for most PPVOs in toluene are between 47 to 60 nm, which is relatively small compared to the NO2-PPVO where the Stokes shift was 97 nm (see Supporting Information Table S1). The Stokes shifts in chloroform become even more drastic, varying from 57 nm for H-PPVO to 201 nm for NO_2-PPVO. We prescribe smaller Stokes shifts as resulting from the dipole−dipole (i.e., solvent-PPVO) interactions, controlled by the difference of ground and excited state permanent dipoles of the substituted PPVO, as well as solvent polarity, constituting the commonly observed solvatochromic effects. In contrast, we attribute the larger Stokes shifts to chromophore aggregation where the close-packed PPVOs have strong intermolecular interactions leading to the appearance of low-lying weakly emitting intermolecular excited states. These aggregated states strongly affect excited states lifetimes and PL quantum yield (QY). For example, the QY of the six PPVOs in toluene, one of the common solvents for all six PPVOs, ranges from 79% for the H-PPVO, 76% for CH_3-PPVO, 68.5% for the COOH-PPVO, 67% for NH_2- and Br-PPVOs, to only 53% for the NO_2-PPVO. The relatively low QY of the NO_2-PPVO suggests formation of aggregated states, which is further supported by comparison between solution and solid state (thin film) PL spectra.

To rationalize the Stokes shifts dependence on the functional group and solvent, we invoke a simple model of solvatochromism, a dipole in a spherical cavity.[36−38] Here the shift of the transition energy in a dielectric medium with respect to vacuum is given by

$$\Delta E = -g(\varepsilon_{static})\frac{\mu\Delta\mu}{a^3} - g(\varepsilon_{optic})\frac{\Delta\mu^2}{2a^3} \quad (1)$$

where a is the cavity radius, μ and $\Delta\mu$ are the molecular permanent dipole moment and its change upon the excitation to S_1 state, $\varepsilon_{static}/\varepsilon_{optic}$ is the static/optical dielectric permittivity of the medium, and

$$g(\varepsilon) = \frac{\varepsilon - 1}{\varepsilon + 1/2} \quad (2)$$

denotes a reaction field factor (because of the reaction field $g(\varepsilon)\mu/a^3$ induced by the dipole). In a given solvent, the spectroscopic shift is proportional to the permanent dipole moment change $|\Delta\mu|$ (eq 1), so the latter (calculated in

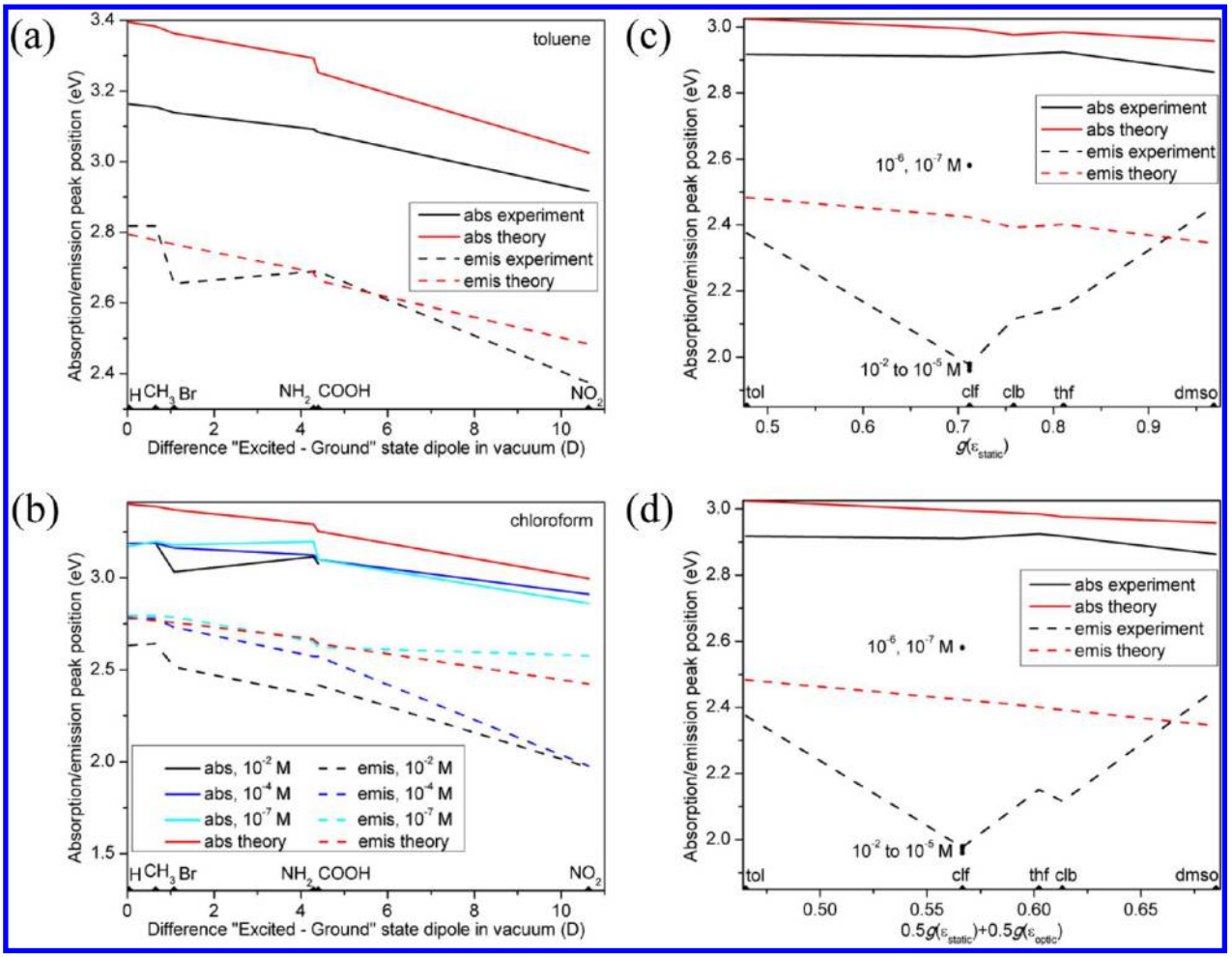

Figure 3. (a, b) First absorption and emission peak positions in toluene (a) and chloroform (b): dependence on the functional group and the concentration. (c, d) The first absorption and emission peak positions for the case of NO_2 group: dependence on the solvent. In panel c, the *x*-axis corresponds to the equilibrium solvation, and in panel d, both equilibrium and nonequilibrium types of solvation are mixed with equal weights. Here the reaction field factor $g(\varepsilon)$ is given by formula 2. For the emission in chloroform, the concentration dependence is shown by dots.

vacuum) was taken as the quantitative descriptor of a functional group. Notably, we observe a steady increase of the permanent dipole moment change $\Delta\mu$ with the rise in electronegativity of the end group, because of enhancement of CT character in the S_1 state leading to a concomitant increase of the excited state dipole moment. Conversely, for a given functional group, the spectroscopic shift (eq 1) is proportional to the weighted sum of $g(\varepsilon_{static})$ and $g(\varepsilon_{optic})$, the quantitative descriptors of a solvent. For the six PPVOs, the dipole in a spherical cavity approximation is only qualitatively correct since the molecular shape is far from spherical and the charge distribution is highly nonuniform. Nevertheless, for both descriptors a monotonic dependence of spectral peak positions is expected.

Using the descriptors defined above, the position of the lowest absorption and emission peaks with respect to a functional group (Figure 3a, b) and solvent (Figure 3c, d) is shown. Both theoretical and experimental results for the absorption are in a good agreement with each other and show appropriate near-linear dependencies on calculated $\Delta\mu$ and $g(\varepsilon)$. Notably, experimental trends are not significantly affected by chromophore concentrations (see Figure 3b). *This observation confirms that for all PPVOs the absorption is dominated by single molecule absorption*; however, the situation becomes more complex for emission. While theoretical data obey the expected near-linear dependencies, the measured emission peak positions show systematic deviations from the calculated ones, which can be interpreted as the onset of aggregation. In particular, in Figure 3b we see a systematic red-shift in the measured emission peak position with an increase in PPVO concentration. At extremely diluted concentrations, the emission is dominated by single molecule emission (as it is clearly seen in Figure 3b), and the measured PL λ_{max} show an excellent agreement with the calculated values. Overall, the aggregation signature depends monotonically on the molecular dipole moment: the larger the moment (Figure 2b), the lower the concentration is required for the emission energy downshift to be observed. The dependence of emission peak position on the solvent polarity (Figure 3c, d) strongly follows eq 1 for quantum-chemical results. However, highly nontrivial non-monotonic dependence appears for measured PL maxima, which signifies strong influence of aggregates on the emission.

Aggregation and PL Spectra. The aggregate-associated change in PL is further validated by the concentration experiments in which we measure PL spectra in diluted PPVO solutions ranging from 10^{-2} to 10^{-7} M (Figure 4a, b). For the NO_2-PPVO in chloroform solution from 10^{-2} to 10^{-4} M concentrations, the PL spectra have a λ_{max} at 632 nm. At 10^{-5} M, we observe the main peak at 632 nm and a shoulder

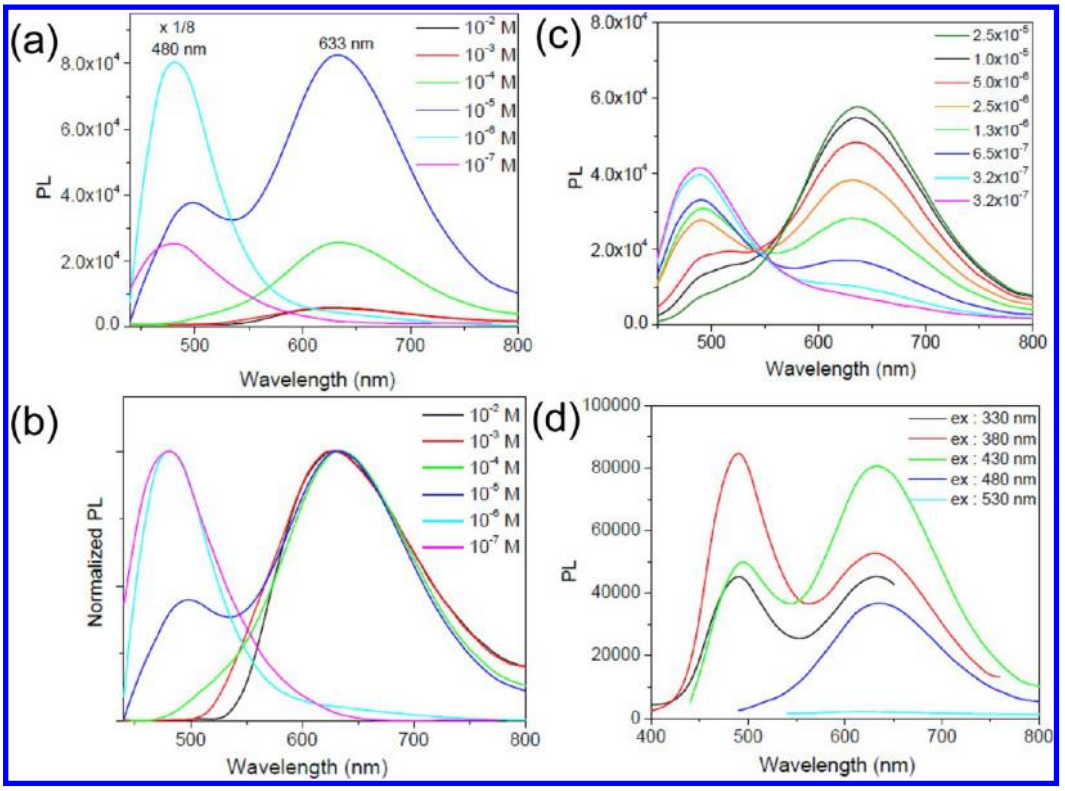

Figure 4. (a) PL spectra of NO_2-PPVO in $CHCl_3$ from 1×10^{-2} to 1×10^{-7} M and (b) the normalized PL spectra. (c) The concentration-dependent PL spectra of NO_2-PPVO in $CHCl_3$ from 2.5×10^{-6} to 1.6×10^{-7} M and (d) excitation wavelength-dependent PL spectra of the 10^{-6} M NO_2-PPVO in $CHCl_3$.

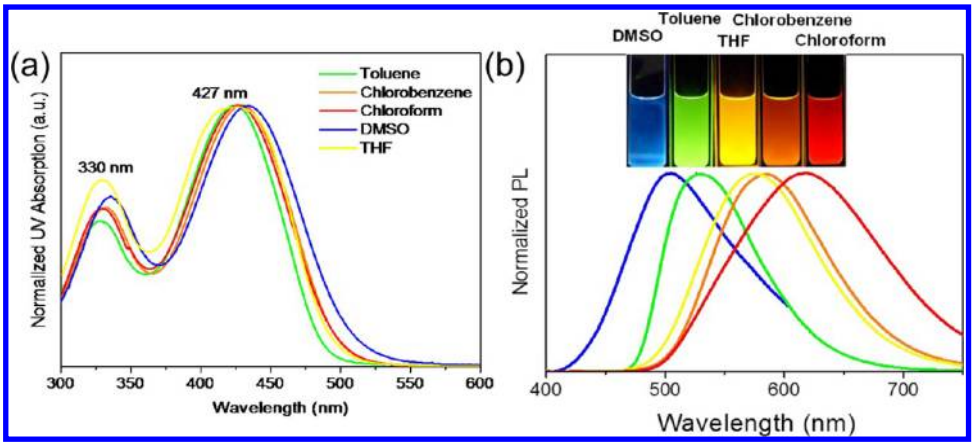

Figure 5. (a) UV–vis and (b) PL spectra of NO_2 trimer in different solvents. Inset is the luminescence color of the trimer solution in different solvents (solvatochromism) which covers the visible spectrum from blue to red.

band at 475 nm. When the concentration reaches 10^{-6} M, the emission peak at 475 nm becomes the dominant feature. Detailed PL spectra measurements (Figure 4c) for concentration ranges from 10^{-5} to 10^{-7} M, illustrate a continuous change in the optical properties manifested by the two distinct emission species suggested by a pseudoisosbestic point. The above results suggest that the peaks at 475 and 632 nm are associated with a single molecule and aggregate emission, respectively. It is important to note that aggregates coexist in all concentrations as evidenced by a weak fluorescence with low QY, compared to the PL QY of the free molecules (Supporting Information Table S1). The NO_2-PPVO aggregates have been detected by dynamic light scattering (DLS) which suggests the presence of aggregates, the size of ~290 nm in chloroform solution under diluted concentration down to 10^{-6} M. This result agrees with the concentration dependent fluorescence spectra, which suggest predominant single molecule species at lower concentrations (<10^{-7} M). Moreover, our results also show that a decrease of solution concentration also leads to reduced volume percent of aggregates in solution.

Another strong evidence of the coexistence of monomers and aggregates in chloroform solution is the excitation dependent PL spectra revealing that monomer and aggregate emission strongly depends on the excitation wavelength (Figure 4d). Upon photoexcitation at 330 nm to the S0–S2 transition for the NO_2-PPVO, both monomer (480 nm) and aggregate (632 nm) emissions are observed with near equal intensity. It appears that there is enough surplus of excitation energy, so

dx.doi.org/10.1021/am400766w | ACS Appl. Mater. Interfaces 2013, 5, 4685–4695

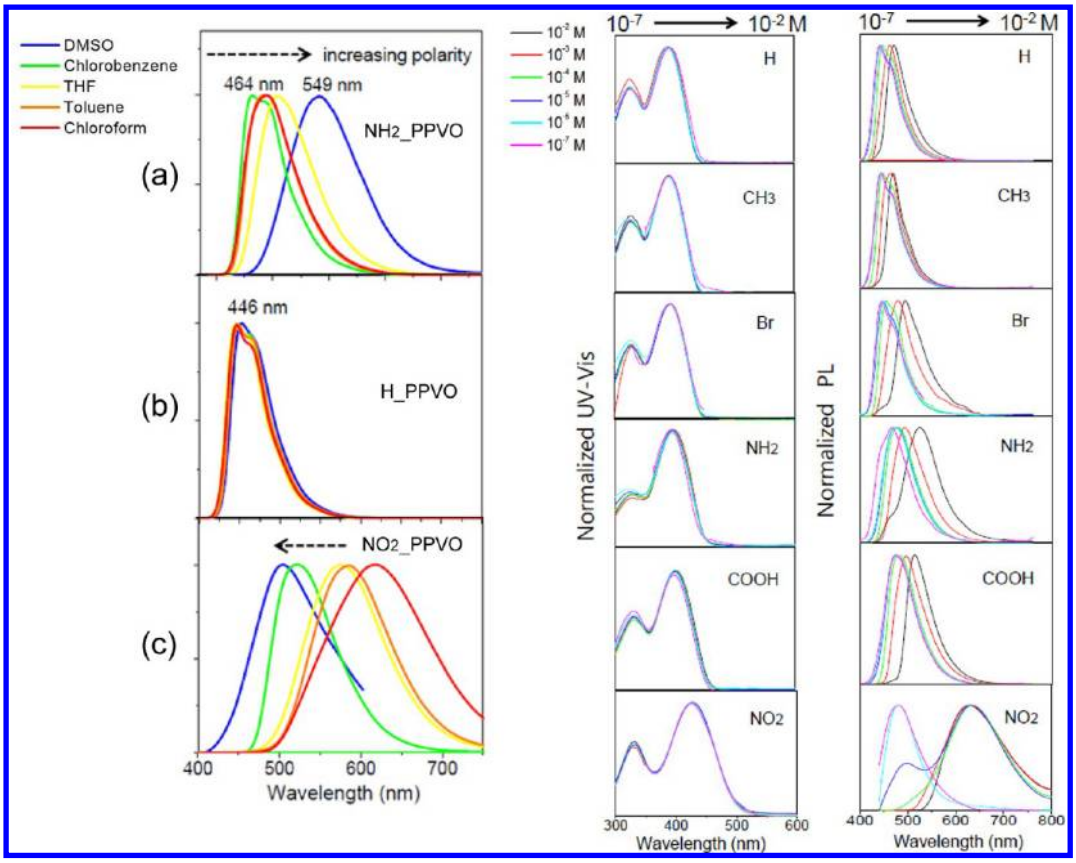

Figure 6. (left) Solvent-dependent fluorescent properties for NH_2-PPVO (a), H-PPVO (b), and NO_2-PPVO (c). (right) Concentration dependent UV−vis and PL spectra for all six PPVOs from 10^{-2} to 10^{-7} M.

that a fraction of the excitations are able to transfer to the low-energy sites related to intermolecular excited states enhancing the aggregate emission. Upon excitation at 380 nm to the S_0-S_1 transition, the PL spectrum is dominated by a monomer emission. However, as we increase the excitation wavelength to 430 nm, toward the edge of monomer absorption, the aggregate emission at 632 nm prevails again, since predominantly only aggregates are excited. Once the excitation wavelength increases to 480 nm, far away from the monomer absorption, we observe only the aggregate emission (Figure 4d). Finally, as the excitation wavelength increases to 530 nm, far away from both the monomer and aggregate emission, the PL vanishes.

One of the most notable optical properties of the NO_2-PPVO is its solvatochromism, which encompasses the entire visible region (from blue to red). Specifically, we observe for the NO_2-terminated PPVO dissolved in DMSO, chloroform, chlorobenzene, toluene, and THF at 5×10^{-6} M the following trends: while the λ_{max} of the absorption spectra for the NO_2-PPVO shows a relatively small change (<20 nm) among all solvents (Figure 5a), the corresponding emission spans the wavelengths from 460 to 630 nm (Figure 5b), encompassing the whole visible spectrum. Such strong solvatochromism occurs due to combination of electrostatic PPVO-solvent interactions intramolecular charge transfer, and aggregate formation in solution. The above result is also consistent with previously reported observations of conjugated oligomers with stronger acceptor end group showing pronounced solvatochromism due to solvent stabilization of intramolecular charge transfer in the excited state.[39]

Finally, Figure 6 summarizes all observed trends in optical spectra of the six PPVOs. The UV−vis absorption spectra (Figure 6, middle column) are insensitive to both the PPVO concentration and solvent polarity; however, they do show some level of dependence on the electronegativity of the end group, with a red shift of λ_{max} and peak broadening for NO_2-PPVO. The broad peaks in the absorption spectra are attributed to conformational disorder (a distribution of torsional angles) and presence of aggregates. Lack of systematic shifts in UV−vis spectra with concentration/solvent polarity reveals that PPVO packing in aggregates is not ordered. Thus, respective electronic couplings cannot be attributed to H- or J-aggregation type. In contrast, the respective PL spectra originating from both single molecules and aggregates show significant sensitivity to solute concentration, solvent polarity and end group electronegativity (Figure 6, right). With an increase of end group electronegativity, the lowest excited state S_1 gains CT character (Figure 3) leading to a PL red-shift. Similarly, PL spectra for the six PPVOs show monotonic red-shifts with an increase in concentration, demonstrating an impact of aggregation. In the case of the NO_2-PPVO, two distinct peaks at 480 and 632 nm manifest single molecule and aggregate emission, respectively. The solvatochromism varies broadly among the six PPVOs (Figure 6, left). Since the H-PPVO does not have a permanent dipole, its fluorescence is dominated by single molecules and the PL shows almost no change with solvent polarity. In contrast, the NH_2-PPVO exhibits red-shifted emission of single molecules with increasing solvent polarity due to stronger stabilization of the excited state by polar solvents (normal solvatochromism). Finally, the solvatochromism for the NO_2-

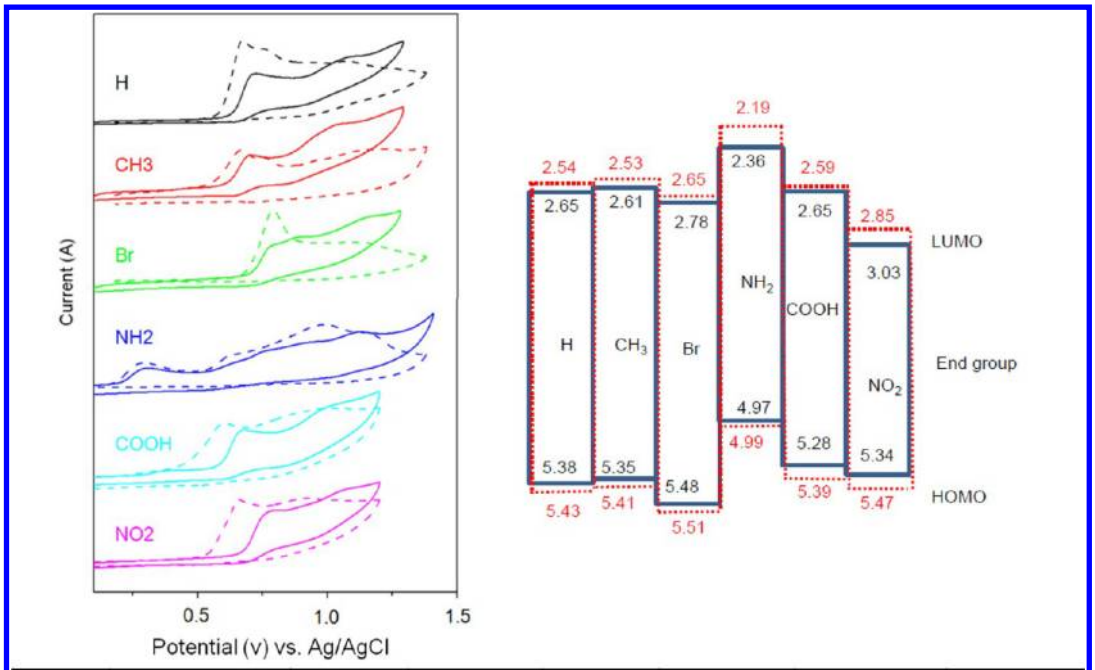

Sample		H_PPVO	CH_3_PPVO	Br_PPVO	NH_2_PPVO	COOH_PPVO	NO_2_PPVO
Solution	Oxidation potential	0.63	0.61	0.71	0.19	0.59	0.67
	HOMO (4.8 + oxidation)	5.43	5.41	5.51	4.99	5.39	5.47
	Band gap (using UV in Toluene solution)	2.89	2.88	2.86	2.80	2.80	2.62
	LUMO	2.54	2.53	2.65	2.19	2.59	2.85
Film	Oxidation potential	0.58	0.55	0.68	0.17	0.48	0.54
	HOMO (4.8 + oxidation)	5.38	5.35	5.48	4.97	5.28	5.34
	Band gap (using UV in film)	2.73	2.74	2.70	2.61	2.63	2.31
	LUMO	2.65	2.61	2.78	2.36	2.65	3.03

Figure 7. Top: (left) Cyclic voltammograms of PPVOs in solution (solid line) and as cast thin film (dashed line), (right) HOMO, LUMO, and band gap energies of PPVOs in solution (red) and as thin films (blue). Bottom: Table listing oxidation potential, HOMO, LUMO, and band gap energy of six PPVOs.

PPVO is drastic and irregular with no monotonic dependence on the solvent polarity (in fact, the most blue-shifted emission is observed in the most polar solvent, DMSO). Solvatochromism of the NO_2-PPVO is attributed to a complex interplay of single molecule and aggregate emission observed for this particular compound.

Redox Potential and Energetics of PPVOs. Cyclic voltammograms (in acetonitrile), the oxidation potential (HOMO), LUMO and bandgap energies of all PPVOs are summarized in Figure 7. Band gap energy is estimated by extrapolating the intersect of tangent lines at the red edge of the absorption peak. The LUMO energies of the PPVOs are obtained by adding HOMO energy with the band gap energy. The oxidation potential of HOMO, LUMO, and band gap energies of all PPVOs are listed in the table in the bottom of Figure 7. The respective calculated values (Figure 2b) show a good agreement with experiment (barring systematic shifts). The oxidation potentials range from 4.97 (NH_2-PPVO) to 5.48 eV (Br-PPVO). The NO_2-PPVO has the smallest bandgap energy and the lowest LUMO energy. All PPVOs exhibit end-group-dependent bandgap energies ranging from 2.31 to 2.74 eV. The delicate change in energetics for PPVOs suggests a valid approach to tailoring the electronic structures of conjugated systems through synthetic chemistry. Such systematic analyses of a series of PPVOs make perfect sense as they were processed in the same solvent which eliminates additional variables induced when more than one solvent is involved. Of all PPVO derivatives, the NH_2-PPVO has the lowest oxidation potential. This exceptionally low oxidation potential is a unique property consistent with the results reported by Hörhold et al. who have shown that in-chain amine groups can dramatically lower the oxidation potentials of the PPV copolymer.[40] Although the exact reason for how the NH_2-substituent lowers the oxidation potential is not clearly understood, Huckel calculations suggest electron density withdrawal from the lone pair on the nitrogen toward the LUMO of benzene rings resulting in a huge HOMO upshift, which further validates our approach to modulate the energetics of the conjugated systems by varying the function/polarity of the end group. Furthermore, if we compare the oxidation potential of these PPVOs to that of

the fullerenes system (PCBM) whose HOMO and LUMO energies are 3.7 and 6.1 eV,[41] respectively, the energetics of our PPVO derivatives ideally match that of the PCBM, hence suggesting their use in photovoltaic (PV) devices. The detailed study of PPVO-based PV devices is currently underway.

Electroluminescence Properties of OPPV Derivatives. To determine how the changes in functional end group impacts the organic light-emitting diode (OLED) performance, non-doped OLED devices were fabricated with the H-, COOH-, and NO_2-PPVO as the emitting material layer. The most important observation is that the electroluminescence (EL) spectra of H-, COOH-, and NO_2-PPVO have λ_{max} at 487, 518, and 587 nm, respectively (see Figure 8). This trend in the EL spectra is in excellent agreement with the end-group dependent PL spectra of the PPVO thin-films. In terms of the Commission Internationale de l'Eclairage (CIE) coordinates, the *x* and *y*-axis values of H-PPVO, NH_2-PPVO, and NO_2-PPVO are (0.16, 0.24), (0.33,0.54), and (0.42, 0.36) that is, closer to the sky blue, green, and red region, respectively (see Figure 8 inset). *These EL spectra and CIE coordinates show that adjusting the molecular dipole by varying the functional group attached to the PPVO changes the optical and electronic properties that are well manifested in OLEDs.* The EL devices in H-, COOH-, and NO_2-PPVO were found to exhibit external quantum efficiencies (EQE) of 0.24% (100 mA/cm^2), 2.77% (10 mA/cm^2), and 0.005% (100 mA/cm^2), respectively. The EQE of COOH-PPVO device is much higher that of H-PPVO and NO_2-PPVO. This difference in EQE can be explained by the following two factors. First, COOH-PPVO has a higher HOMO level (5.28 eV) compared to H-PPVO (5.38 eV) and NO_2-PPVO (5.34 eV), allowing for a better hole injection in OLED devices. Second, the EL device of COOH-PPVO has more favorable charge balance than the devices prepared from H and NO_2-PPVO.

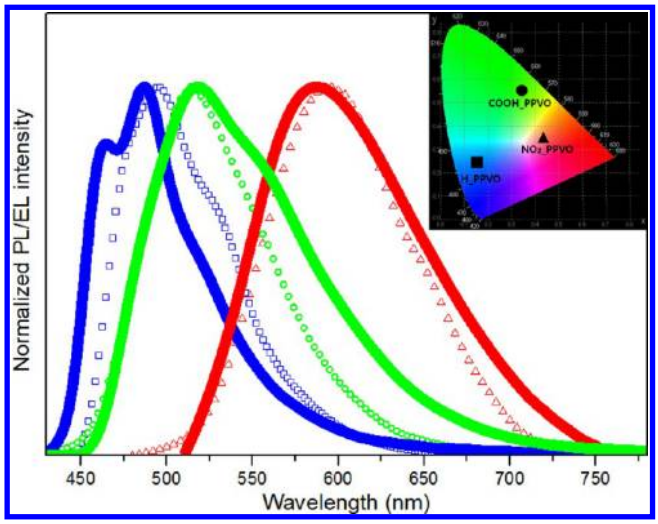

Figure 8. Normalized PL spectra in PPVO thin films (symbol) and EL spectra (line) of H-PPVO (blue), COOH-PPVO (green), and NO_2-PPVO (red). Insets show the CIE value in the OLED device.

CONCLUSIONS

We have prepared a series of *para*-phenylene vinylene oligomers with end groups that vary in their electronegativity, which leads to structure-dependent optical, electronic, and redox properties. Our experimental characterization and complementary electronic structure modeling reveal strong correlations between the substituents and electronic properties in solution and solid state, including absorption, emission, and redox potentials. UV−vis absorption spectra of all molecules dominated by two strongly allowed $\pi-\pi^*$ electronic transitions of single molecules, are moderately affected by the solvent polarity and electronegativity of the end group. In contrast, the latter strongly effect the emission wavelengths and efficiency. Moreover, our results suggest the deterministic role of aggregates in the optical properties of the solutions and thin films. For example, the NO_2-PPVO has the strongest permanent dipole and contains both the single molecule and aggregate species in chloroform. This compound has solvent-dependent optical properties (solvatochromism) ranging from blue to red color, thus, encompassing the entire visible spectrum. The electroluminescence (EL) spectra of H-, COOH-, and NO_2-PPVO in OLED devices have λ_{max} at 487, 518, and 587 nm, respectively. This trend in the EL spectra is in excellent agreement with the end group-dependent PL spectra of the PPVO thin-films. Thus, the wide range of spectral shifts observed across the PPVO suite is resulting from the complex interplay between dipole−dipole interactions, aggregate formation, and electronic structure, originated from the difference in end group electronegativity. In particular, the amine end group exhibits the lowest oxidation potential, which corresponds to the HOMO energy level, suggesting a way to lower the oxidation potential with implications for LEDs and photovoltaic applications.

ASSOCIATED CONTENT

Supporting Information

^{1}H, ^{13}C NMR, FT-IR, XRD spectra, and conformational analysis of PPVO derivatives, UV−vis absorption, photoluminescence, Stokes shift, and quantum yield of all six PPVOs on chloroform and toluene, list of all media used in the theoretical calculations, their abbreviations, and values of static and optical dielectric constant, and PL spectra of NO_2-PPVO in chloroform solution under front face geometry. This information is available free of charge via the Internet at http://pubs.acs.org/.

AUTHOR INFORMATION

Corresponding Author

*E-mail: hwang@lanl.gov (H.-L.W.); serg@lanl.gov (S.T.).

Notes

The authors declare no competing financial interest.

ACKNOWLEDGMENTS

We acknowledge support of the Basic Energy Science (BES), Materials Sciences and Engineering Division, Biomolecular Materials program, U.S. Department of Energy and Los Alamos National Laboratory (LANL) Directed Research and Development Funds. Los Alamos National Laboratory is operated by Los Alamos National Security, LLC, for the National Nuclear Security Administration of the U.S. Department of Energy under contract DE-AC52-06NA25396. We acknowledge support of the Center for Integrated Nanotechnologies (CINT), a DOE Nanoscience User Facility, and the Center for Nonlinear Studies (CNLS).

REFERENCES

(1) Cornil, J.; Beljonne, D.; Friend, R. H.; Bredas, J. L. *Chem. Phys. Lett.* **1994**, *223*, 82.
(2) Burroughes, J. H.; Bradley, D. D. C.; Brown, A. R.; Marks, R. N.; Mackay, K.; Friend, R. H.; Burns, P. L.; Holmes, A. B. *Nature* **1990**, *347*, 539.
(3) Segura, J. L.; Martin, N.; Guldi, D. M. *Chem. Soc. Rev.* **2005**, *34*, 31.
(4) Heeger, A. J. *Chem. Soc. Rev.* **2010**, *39*, 2354.
(5) Sun, Y. M.; Welch, G. C.; Leong, W. L.; Takacs, C. J.; Bazan, G. C.; Heeger, A. *Nat. Mater.* **2012**, *11*, 44.
(6) Dou, L. T.; You, J. B.; Yang, J.; Chen, C. C.; He, Y. J.; Murase, S.; Moriarty, T.; Emery, K.; Li, G.; Yang, Y. *Nat. Photonics* **2012**, *6*, 180.
(7) Mukamel, S.; Tretiak, S.; Wagersreiter, T.; Chernyak, V. *Science* **1997**, *277*, 781.
(8) Koller, G.; Berkebile, S.; Oehzelt, M.; Puschnig, P.; Ambrosch-Draxl, C.; Netzer, F. P.; Ramsey, M. G. *Science* **2007**, *317*, 351.
(9) van Hutten, P. F.; Wildeman, J.; Meetsma, A.; Hadziioannou, G. *J. Am. Chem. Soc.* **1999**, *121*, 5910.
(10) Bazan, G. C.; Oldham, W. J.; Lachicotte, R. J.; Tretiak, S.; Chernyak, V.; Mukamel, S. *J. Am. Chem. Soc.* **1998**, *120*, 9188.
(11) Nielsen, C. B.; Angerhofer, A.; Abboud, K. A.; Reynolds, J. R. *J. Am. Chem. Soc.* **2008**, *130*, 9734.
(12) Nguyen, T. Q.; Doan, V.; Schwartz, B. J. *J. Chem. Phys.* **1999**, *110*, 4068.
(13) Schwartz, B. J. *Annu. Rev. Phys. Chem.* **2003**, *54*, 141.
(14) Scherf, U. *Carbon Rich Compounds II*; Springer: Berlin, 1999; Vol. *201*, p 163.
(15) Banerjee, M.; Shukla, R.; Rathore, R. *J. Am. Chem. Soc.* **2009**, *131*, 1780.
(16) Chen, T. A.; Wu, X. M.; Rieke, R. D. *J. Am. Chem. Soc.* **1995**, *117*, 233.
(17) Wautelet, P.; Moroni, M.; Oswald, L.; LeMoigne, J.; Pham, A.; Bigot, J. Y.; Luzzati, S. *Macromolecules* **1996**, *29*, 446.
(18) Ellinger, S.; Graham, K. R.; Shi, P. J.; Farley, R. T.; Steckler, T. T.; Brookins, R. N.; Taranekar, P.; Mei, J. G.; Padilha, L. A.; Ensley, T. R.; Hu, H. H.; Webster, S.; Hagan, D. J.; Van Stryland, E. W.; Schanze, K. S.; Reynolds, J. R. *Chem. Mater.* **2011**, *23*, 3805.
(19) Yang, C.; Cho, S.; Chiechi, R. C.; Walker, W.; Coates, N. E.; Moses, D.; Heeger, A. J.; Wudl, F. *J. Am. Chem. Soc.* **2008**, *130*, 16524.
(20) Horie, M.; Kettle, J.; Yu, C. Y.; Majewski, L. A.; Chang, S. W.; Kirkpatrick, J.; Tuladhar, S. M.; Nelson, J.; Saunders, B. R.; Turner, M. L. *J. Mater. Chem.* **2012**, *22*, 381.
(21) Ajayaghosh, A. *Chem. Soc. Rev.* **2003**, *32*, 181.
(22) Ahmed, E.; Ren, G. Q.; Kim, F. S.; Hollenbeck, E. C.; Jenekhe, S. A. *Chem. Mater.* **2011**, *23*, 4563.
(23) Roncali, J. *Acc. Chem. Res.* **2000**, *33*, 147.
(24) Frisch, M. J.; Trucks, G. W.; Schlegel, H. B.; Scuseria, G. E.; Robb, M. A.; Cheeseman, J. R.; Scalmani, G.; Barone, V.; Mennucci, B.; Petersson, G. A.; Nakatsuji, H.; Caricato, M.; Li, X.; Hratchian, H. P.; Izmaylov, A. F.; Bloino, J.; Zheng, G.; Sonnenberg, J. L.; Hada, M.; Ehara, M.; Toyota, K.; Fukuda, R.; Hasegawa, J.; Ishida, M.; Nakajima, T.; Honda, Y.; Kitao, O.; Nakai, H.; Vreven, T.; Montgomery, J. A., Jr.; Peralta, J. E.; Ogliaro, F.; Bearpark, M.; Heyd, J. J.; Brothers, E.; Kudin, K. N.; Staroverov, V. N.; Kobayashi, R.; Normand, J.; Raghavachari, K.; Rendell, A.; Burant, J. C.; Iyengar, S. S.; Tomasi, J.; Cossi, M.; Rega, N.; Millam, J. M.; Klene, M.; Knox, J. E.; Cross, J. B.; Bakken, V.; Adamo, C.; Jaramillo, J.; Gomperts, R.; Stratmann, R. E.; Yazyev, O.; Austin, A. J.; Cammi, R.; Pomelli, C.; Ochterski, J. W.; Martin, R. L.; Morokuma, K.; Zakrzewski, V. G.; Voth, G. A.; Salvador, P.; Dannenberg, J. J.; Dapprich, S.; Daniels, A. D.; Farkas, O.; Foresman, J. B.; Ortiz, J. V.; Cioslowski, J.; Fox, D. J. *Gaussian 09*, revision A.1; Gaussian, Inc.: Wallingford, CT, 2009.
(25) Yanai, T.; Tew, D. P.; Handy, N. C. *Chem. Phys. Lett.* **2004**, *393*, 51.
(26) Magyar, R. J.; Tretiak, S. *J. Chem. Theory Comput.* **2007**, *3*, 976.
(27) Nayyar, I. H.; Batista, E. R.; Tretiak, S.; Saxena, A.; Smith, D. L.; Martin, R. L. *J. Phys. Chem. Lett.* **2011**, *2*, 566.
(28) Badaeva, E.; Harpham, M. R.; Guda, R.; Süzer, O. z. n.; Ma, C.-Q.; Bäuerle, P.; Goodson, T.; Tretiak, S. *J. Phys. Chem. B* **2010**, *114*, 15808.
(29) Masunov, A.; Tretiak, S. *J. Phys. Chem. B* **2003**, *108*, 899.
(30) Badaeva, E. A.; Timofeeva, T. V.; Masunov, A.; Tretiak, S. *J. Phys. Chem. A* **2005**, *109*, 7276.
(31) Takano, Y.; Houk, K. N. *J. Chem. Theory Comput.* **2004**, *1*, 70.
(32) Cossi, M.; Rega, N.; Scalmani, G.; Barone, V. *J. Comput. Chem.* **2003**, *24*, 669.
(33) Martin, R. L. *J. Chem. Phys.* **2003**, *118*, 4775.
(34) Jacobs, S.; Eevers, W.; Verreyt, G.; Geise, H. J.; Degroot, A.; Dommisse, R. In *Symposium on Molecular Electronics: Doping and Recognition in Nanostructured Materials of the E-MRS Spring Conference*, 19930504−19930507, Strasbourg, France, 1−2 ed.; Elsevier Science: Lausanne, Switzerland; Vol. *61*, pp 189−193.
(35) Rappoport, D.; Furche, F. *Time-Dependent Density Functional Theory*; Marques, M., Ullrich, C., Nogueira, F., Rubio, A., Burke, K., Gross, E., Eds.; Springer: Berlin, 2006; Vol. *706*, pp 337−354.
(36) Reichardt, C.; Welton, T. *Solvents and Solvent Effects in Organic Chemistry*; Wiley-VCH: Weinheim, Germany, 2011.
(37) Improta, R.; Barone, V.; Scalmani, G.; Frisch, M. J. *J. Chem. Phys.* **2006**, *125*, No. 054103.
(38) Tomasi, J.; Mennucci, B.; Cammi, R. *Chem. Rev.* **2005**, *105*, 2999.
(39) Woo, H. Y.; Liu, B.; Kohler, B.; Korystov, D.; Mikhailovsky, A.; Bazan, G. C. *J. Am. Chem. Soc.* **2005**, *127*, 14721.
(40) Rost, H.; Teuschel, A.; Pfeiffer, S.; Horhold, H. H. *Synth. Met.* **1997**, *84*, 269.
(41) Meijer, E. J.; De Leeuw, D. M.; Setayesh, S.; Van Veenendaal, E.; Huisman, B. H.; Blom, P. W. M.; Hummelen, J. C.; Scherf, U.; Klapwijk, T. M. *Nat. Mater.* **2003**, *2*, 678.

Supplemental information

Tailored electronic structure and optical properties of conjugated systems through aggregates and dipole-dipole interactions

Young Il Park, Cheng-Yu Kuo, Yong-Shin Park, Jennifer S. Martinez, Olena Postupna, Andriy Zhugayevych, Seungho Kim, Jongwook Park, Sergei Tretiak, Hsing-Lin Wang

Contents

1. ^{1}H and ^{13}C NMR data of PPVO derivatives

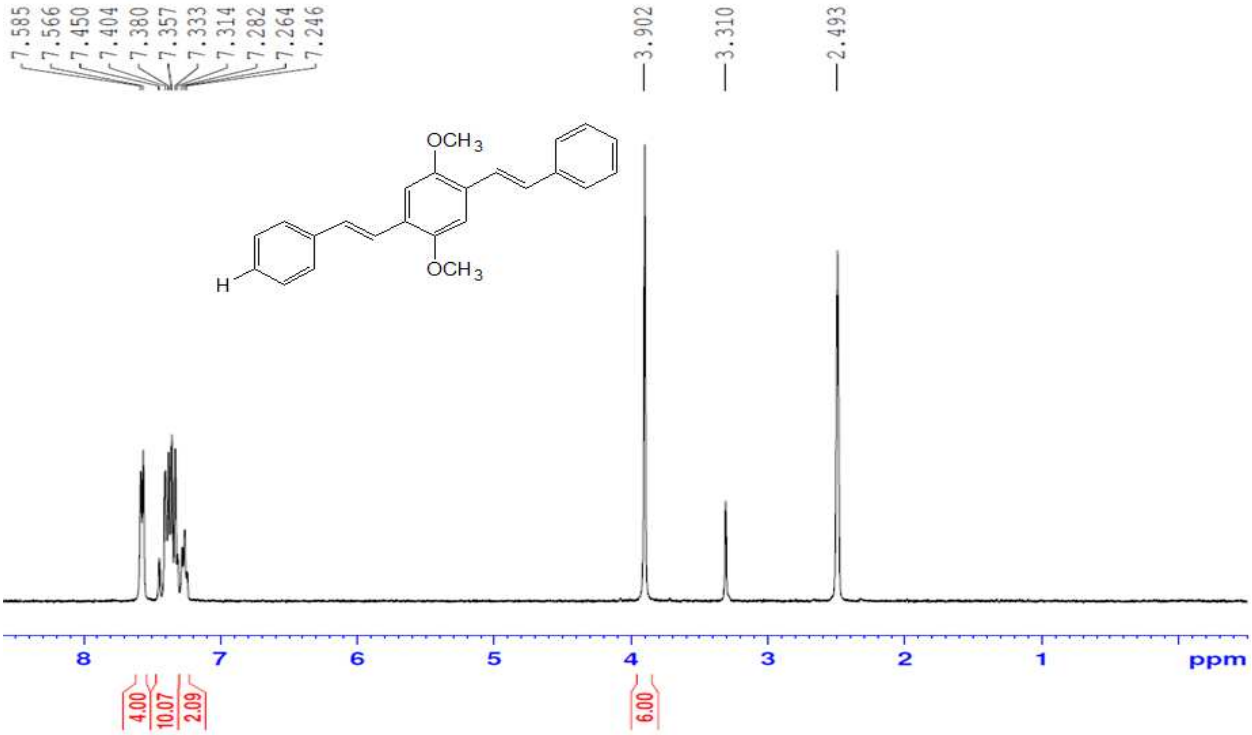

^{1}H-NMR of H_PPVO

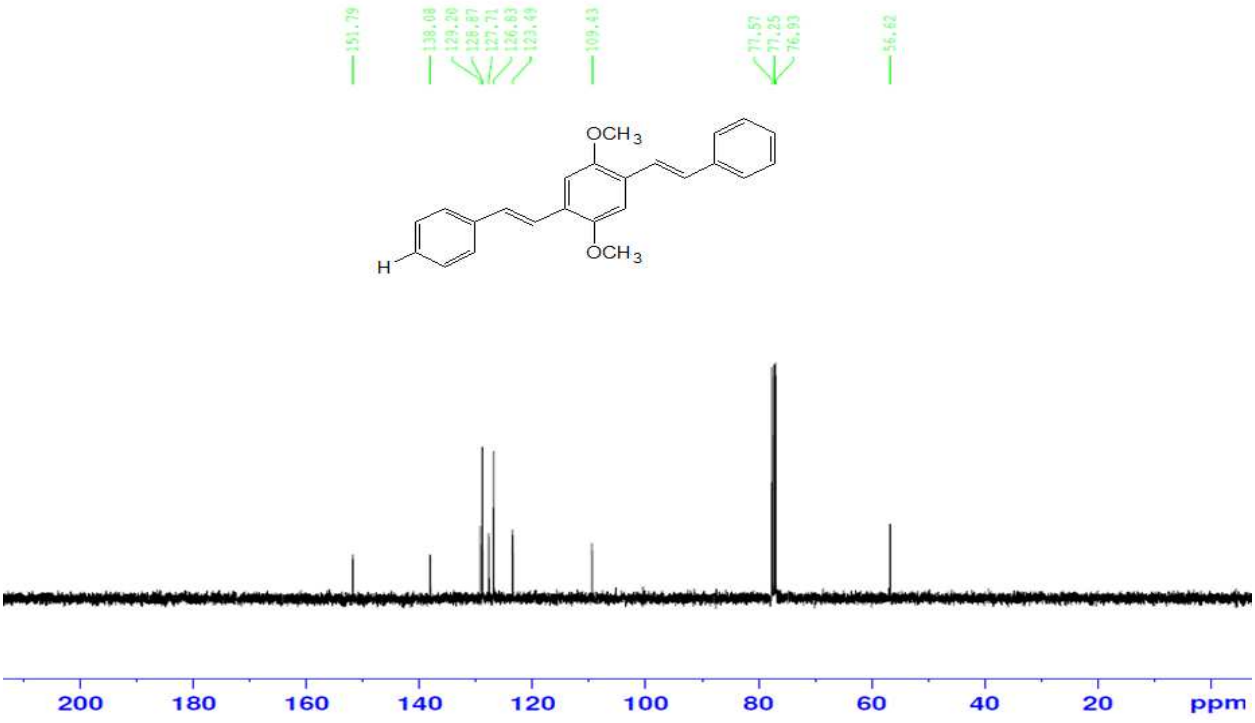

^{13}C-NMR of H_PPVO

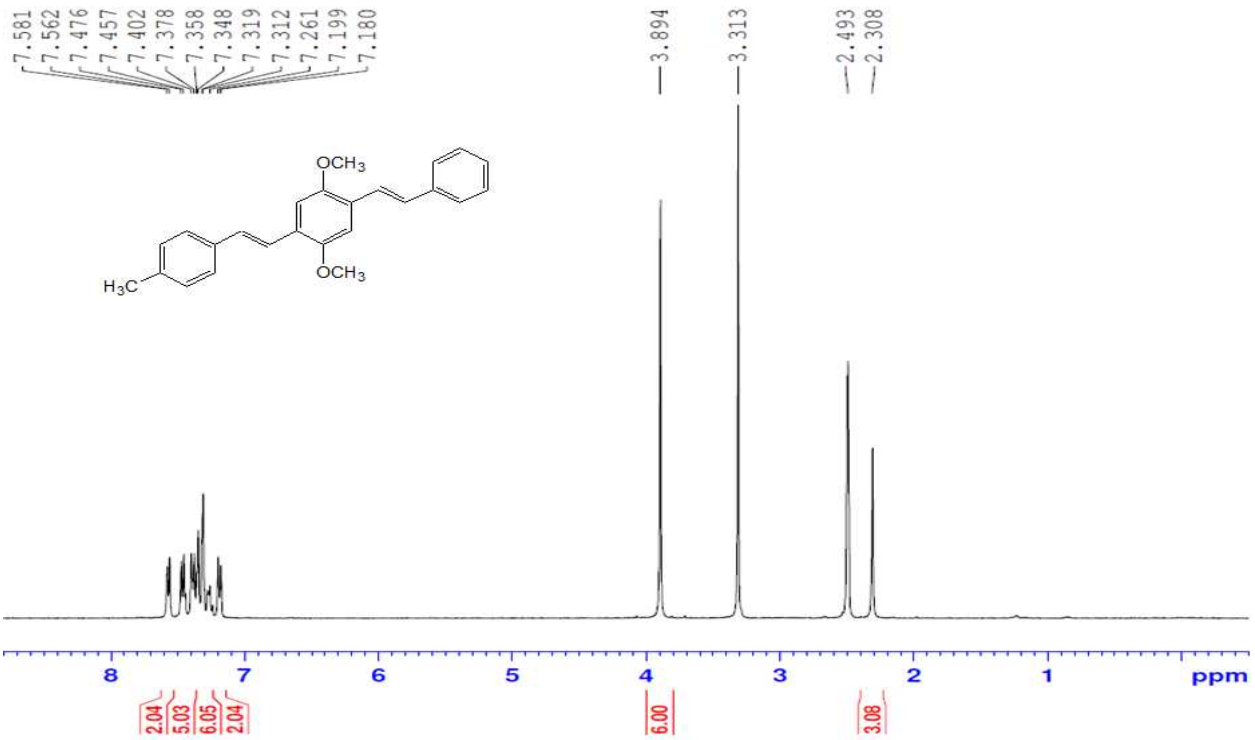

^{1}H-NMR of CH3_PPVO

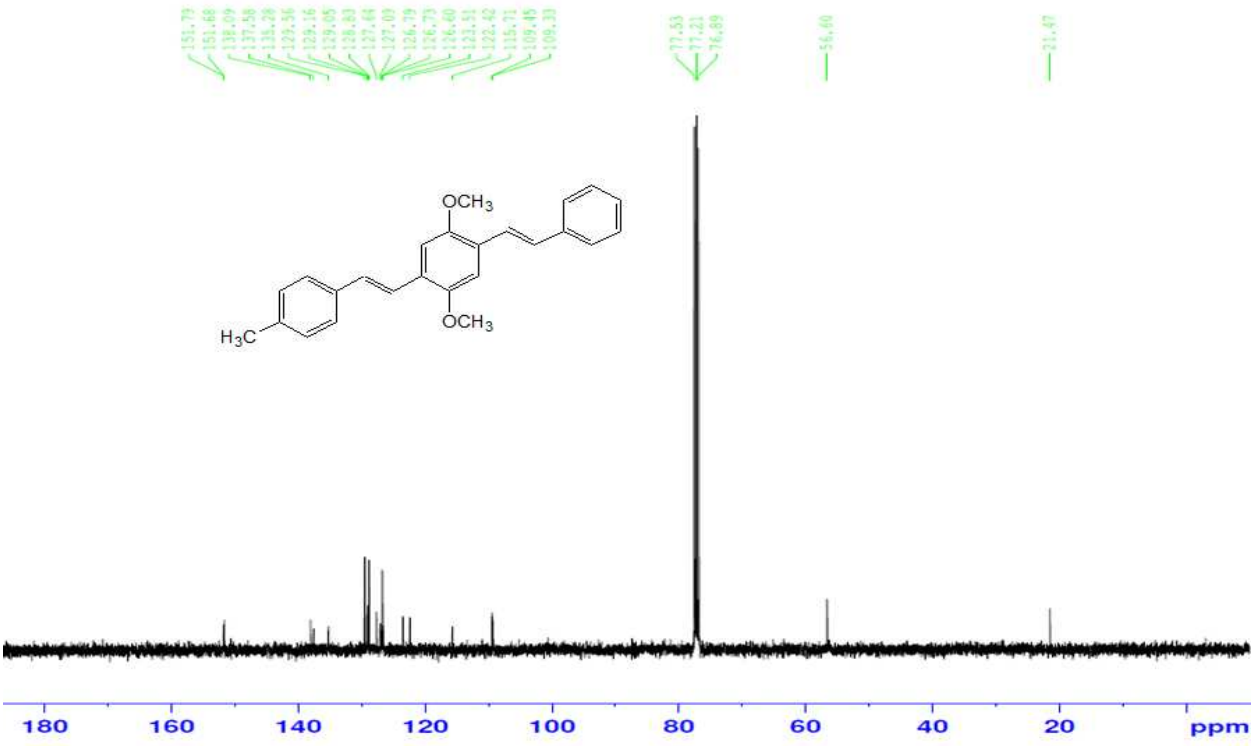

^{13}C-NMR of CH3_PPVO

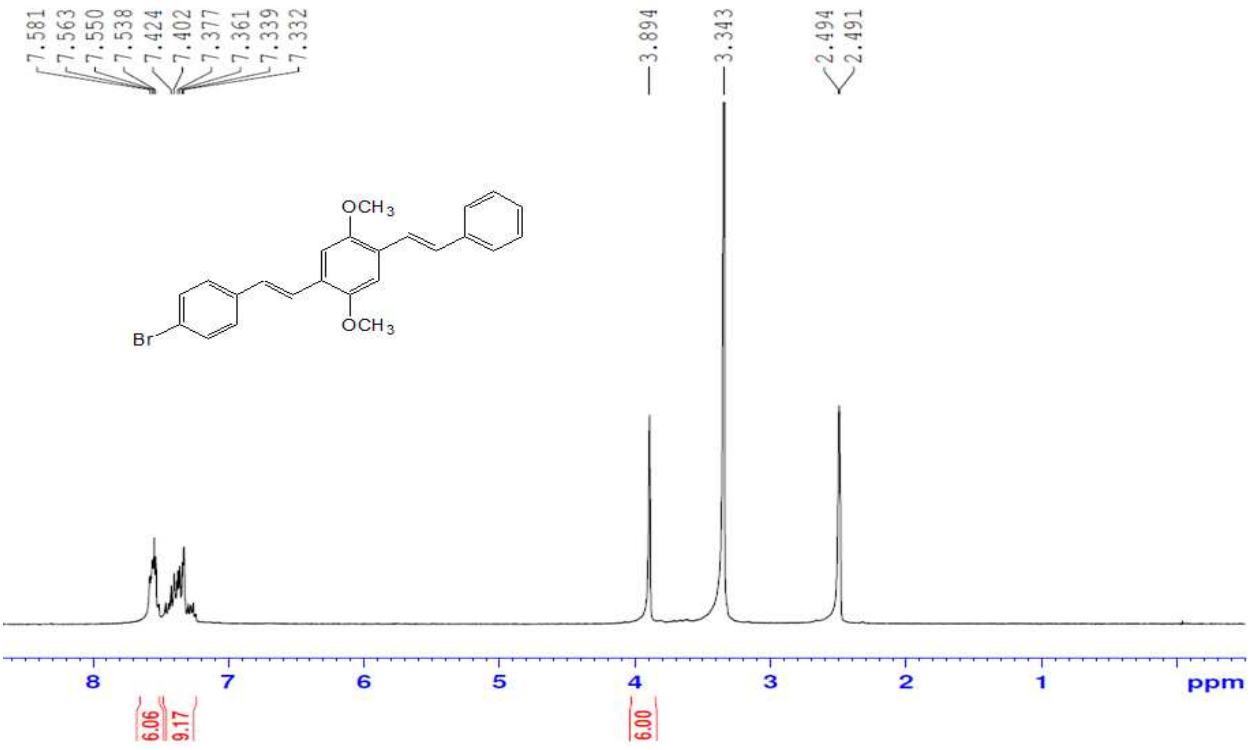

^{1}H-NMR of Br_PPVO

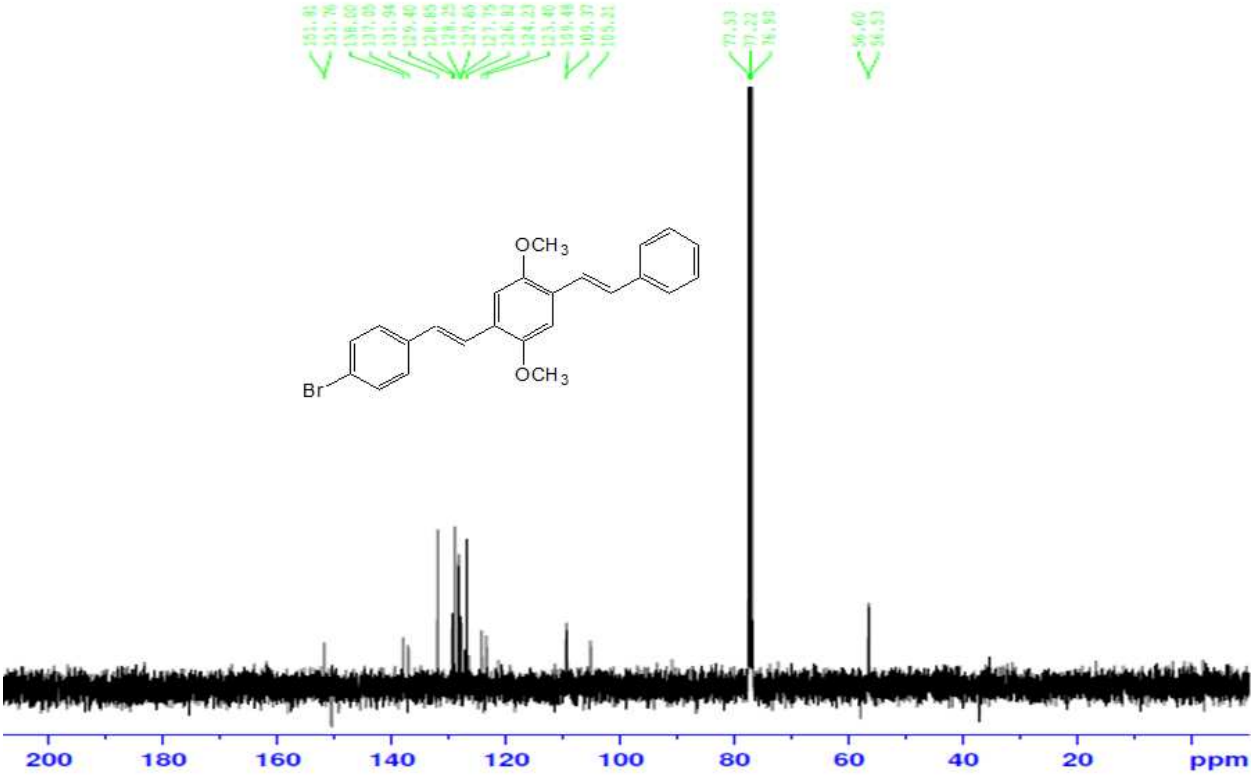

^{13}C-NMR of Br_PPVO

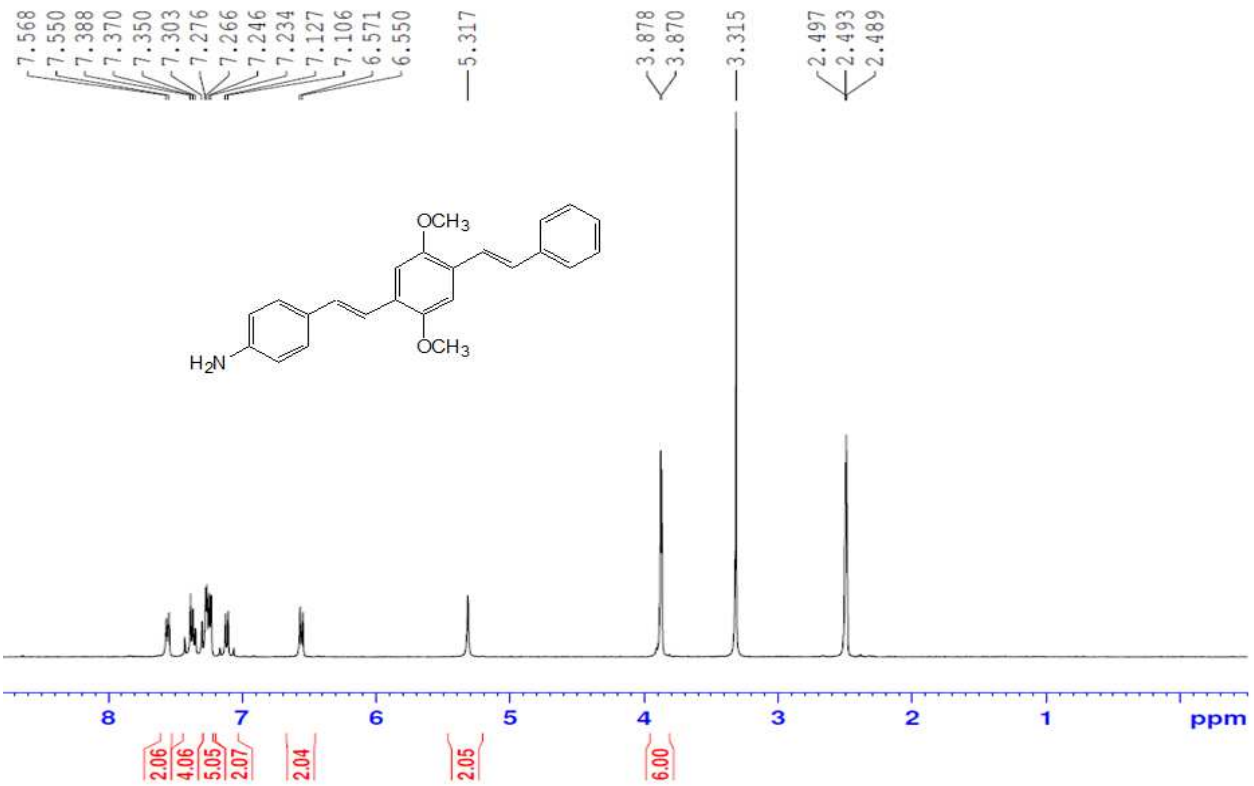

^{1}H-NMR of NH_2_PPVO

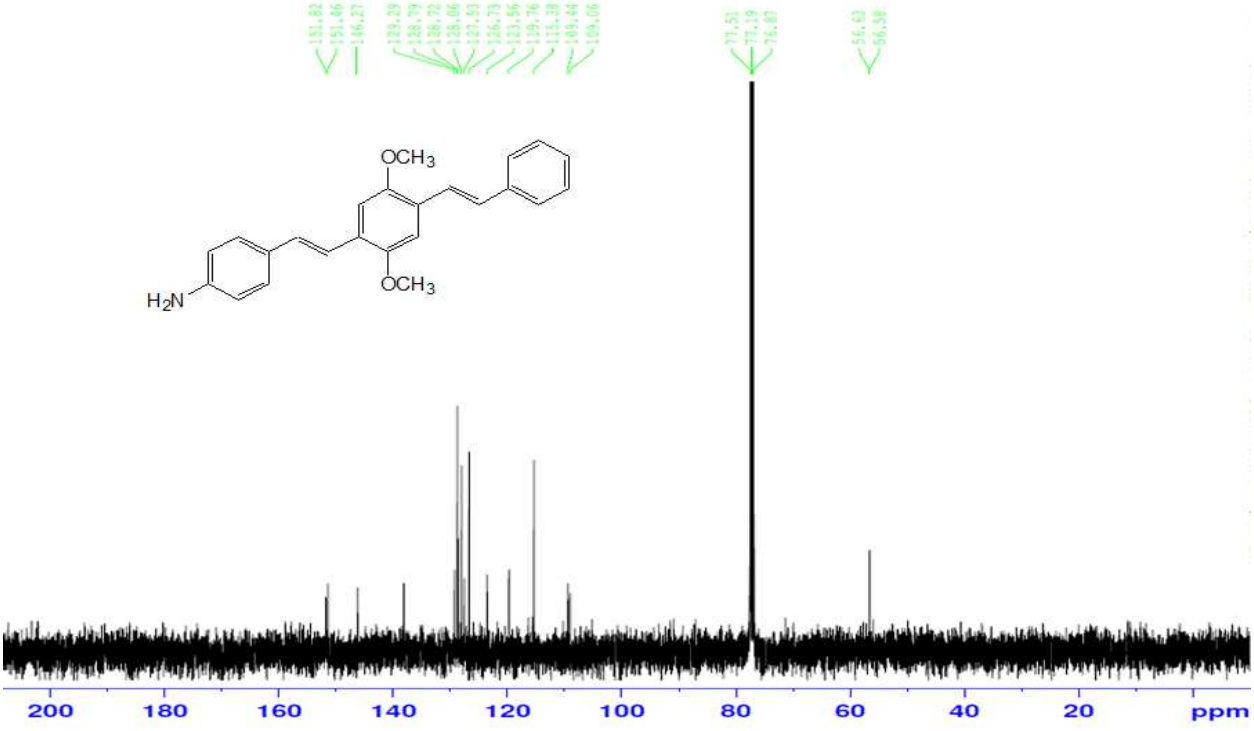

^{13}C-NMR of NH_2_PPVO

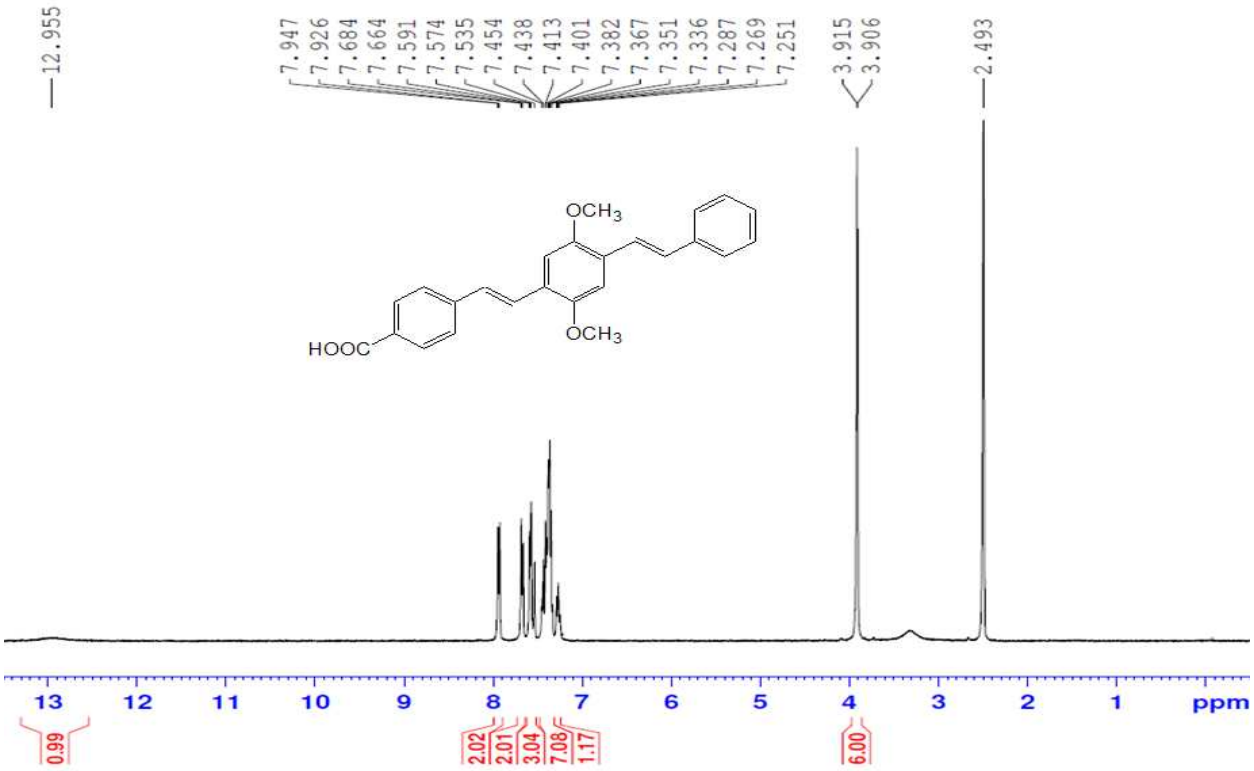

^{1}H-NMR of COOH_PPVO

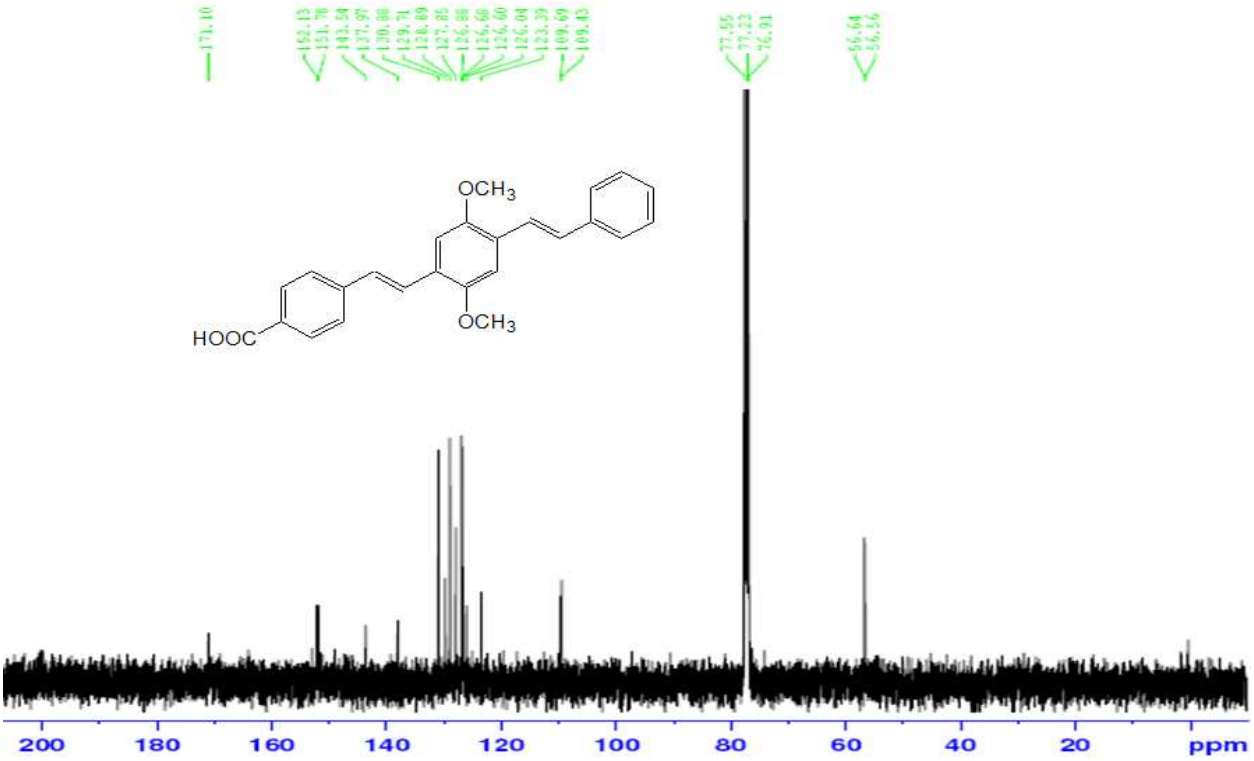

^{13}C-NMR of COOH_PPVO

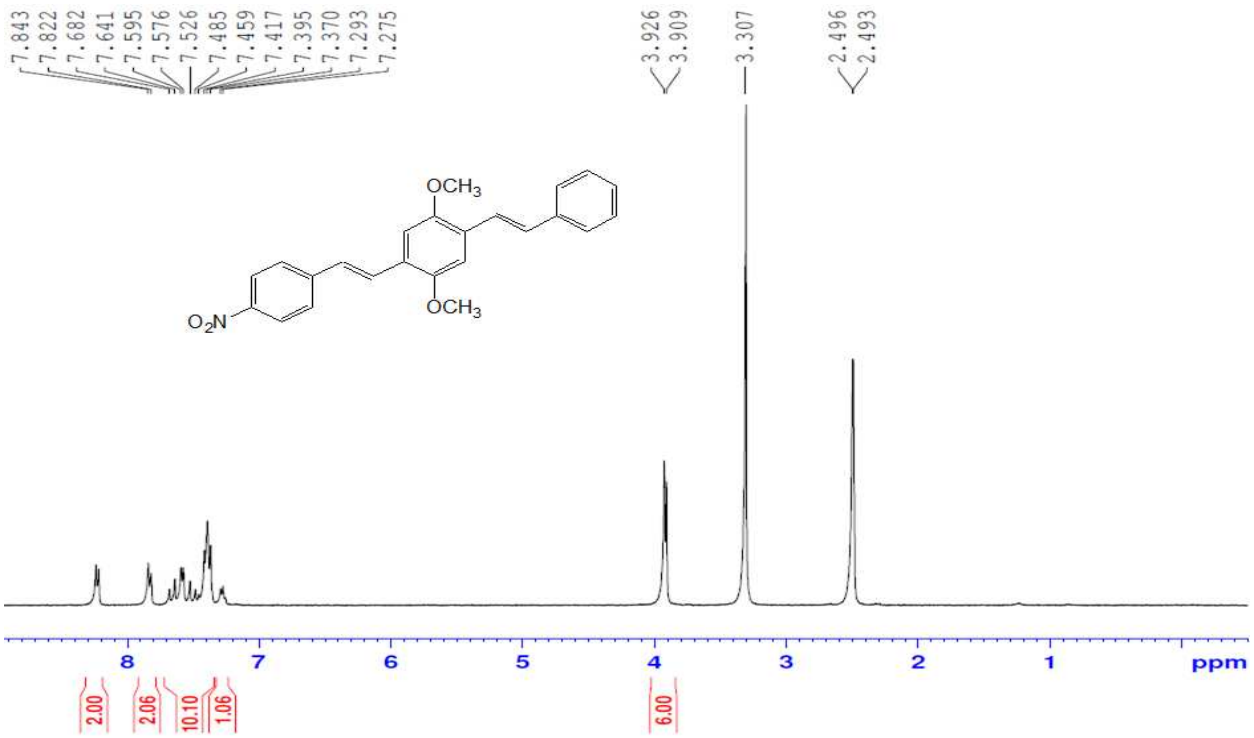

^{1}H-NMR of NO2_PPVO

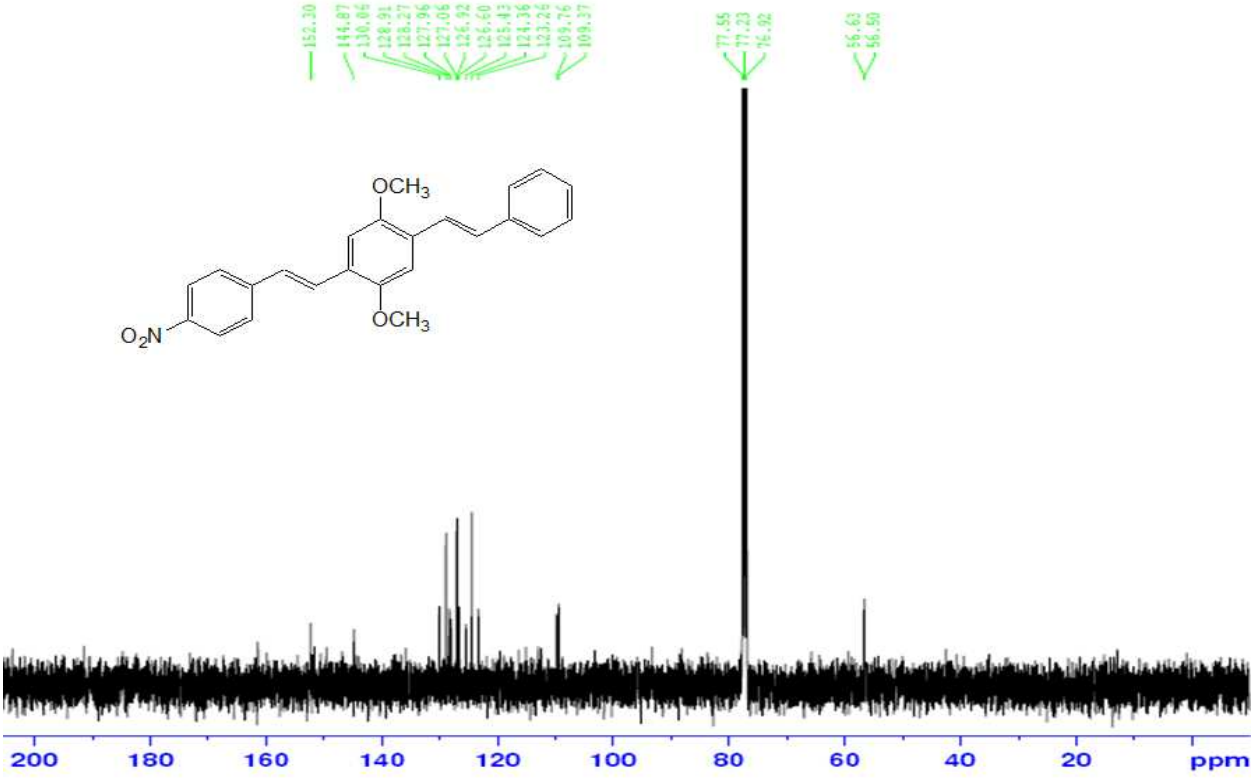

^{13}C-NMR of NO2_PPVO

2. Conformational analysis

Molecular dynamics (MD) simulations with TINKER [J. W. Ponder, TINKER 6.0, http://dasher.wustl.edu/tinker/] using the MM3 force field [N. L. Allinger et al, J. Comput. Chem. 11, 868 (1990)] were carried out to discover alternative conformations. For most of the molecules at room temperature within 100 ps of the simulation time, a 360-degree rotation of the benzene rings and the interconnecting vinyl groups is observed. A few conformations with energies spread over 0.1 eV, were obtained by optimizing the MD snapshots. A conformation with an inverted vinyl group (Fig. 5S) was studied by ab-initio methods. The calculated absorption spectrum differs insignificantly (less than 10 nm) from that of the ground state conformation. Consequently, only the lowest energy conformation is used for further investigation.

		H_PPVO	CH_3_PPVO	Br_PPVO	NH_2_PPVO	COOH_PPVO	NO_2_PPVO
Solution (Toluene)	UV	392	393	395	401	402	425
	PL	440	440	467	461	461	522
Stock Shift in solution		48	47	72	60	59	97
Solution ($CHCl_3$)	UV	389	389	392	397	400	426
	PL	446	446	454	482	482	627
Stock Shift in solution		57	57	62	85	82	201
Film	UV	406	401	391	412	413	445
	PL	494	480	496	516	514	596
Stock Shift in film		88	79	105	104	101	151
PL (Film – Solution(Toluene))		54	40	29	55	53	74
Film	HOMO	5.39	5.36	5.48	4.98	5.20	5.51
	LUMO	2.66	2.62	2.78	2.37	2.57	3.20
Q.Y.		0.89	0.90	0.89	0.29	0.79	0.01

Table S1. List of λ_{max}, for UV-Vis absorption, photoluminescence, Stokes shift and quantum yield of all six PPVOs. These results reveal a strong correlation between the molecular dipole and optical properties. Such correlations are interpreted as due to strong molecular solvent interactions and the formation of various aggregates as manifested by the light scattering

Media	abbr	ε_{static}	$\varepsilon_{optical}$
Toluene	tol	2.37	2.24
Chloroform	clf	4.71	2.09
Chlorobenzene	clb	5.70	2.32
Tetrahydrofuran	thf	7.43	1.97
Acetonitrile	an	35.69	1.81
Dimethyl sulfoxide	dmso	46.83	2.01

Table S2: List of all the media used in the theoretical calculations, their abbreviations and values of static and optical dielectric constants.

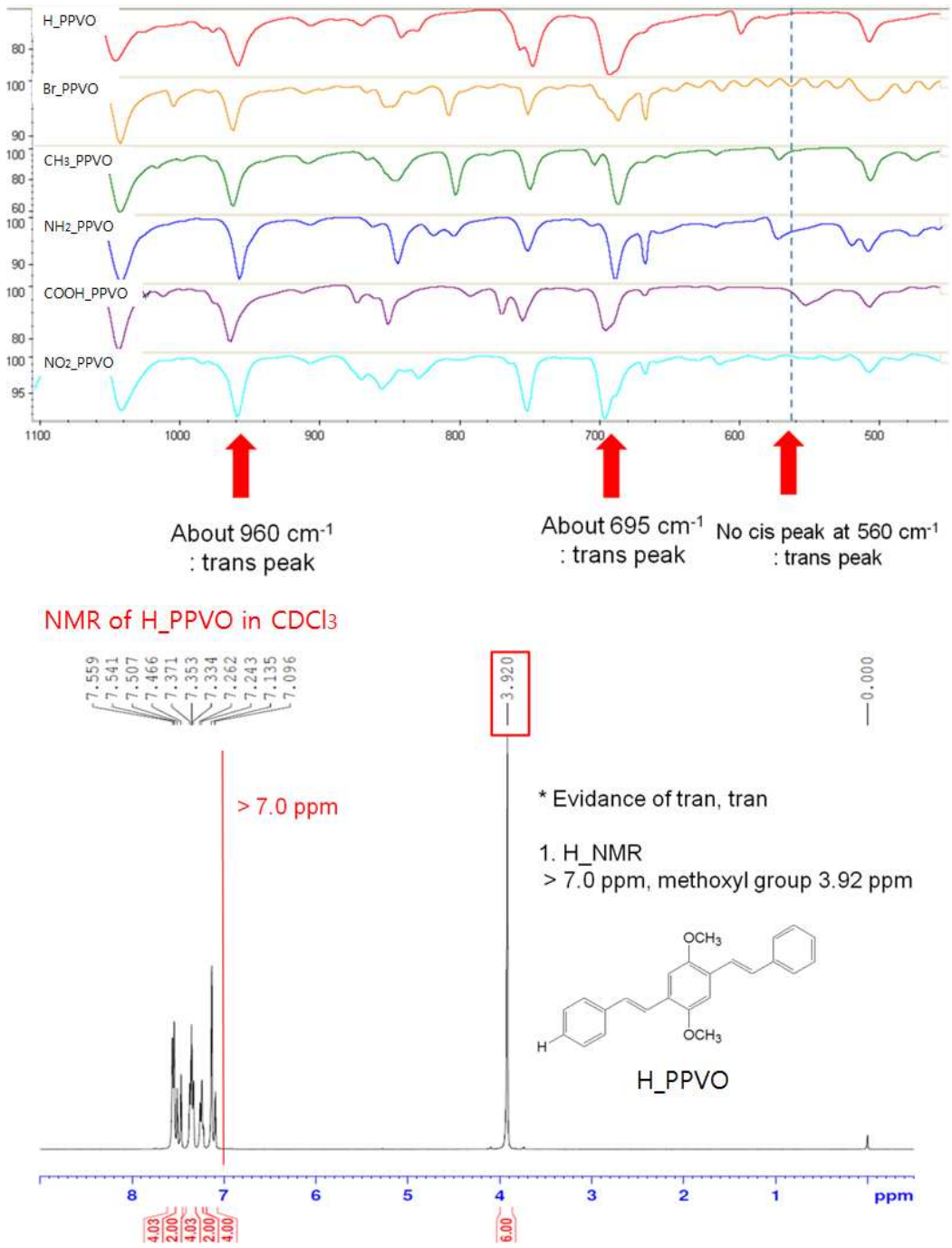

Figure S1. (Top) FT-IR spectra of all six PPVOs. Two peaks at 960 cm^{-1} and 695 cm^{-1} reveal only *trans- trans* conformation in all six PPVOs. Lacking the leak at ~ 560 cm^{-1} suggest that no *cis-trans*, and *cis-cis* conformations. (Bottom) NMR spectrum of H-PPVO shows that all aromatic protons have a chemical shift above 7.0 ppm further validates the fact that only *trans-trans* conformation in the H PPVO. In fact, the chemical shifts of all six PPVOs have aromatic proton greater than 7.0 ppm (see experimental section).

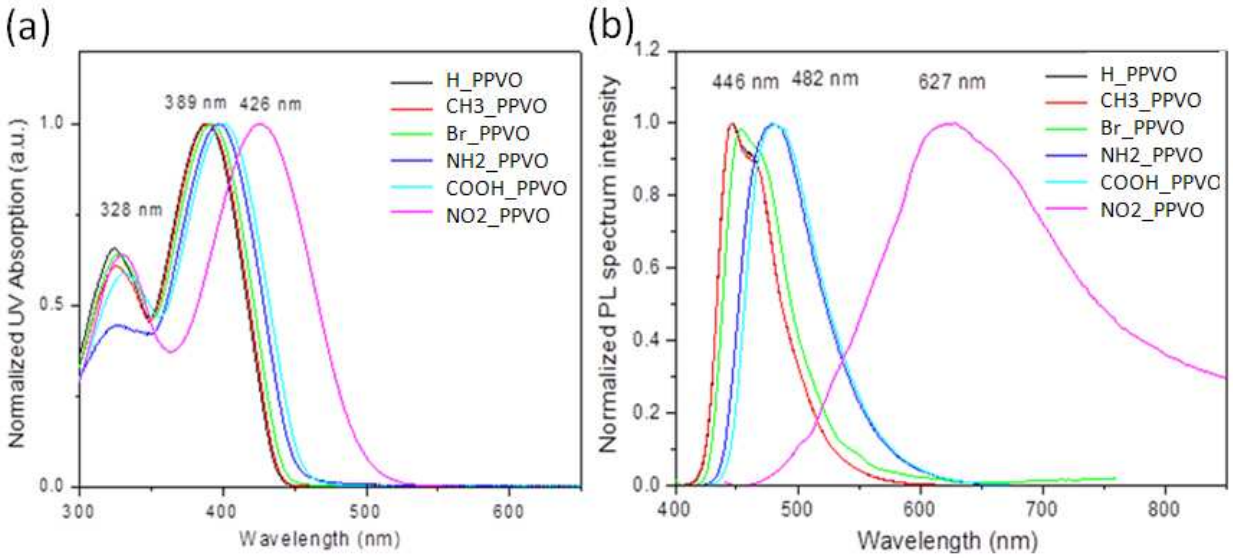

Figure S2. UV-Vis spectra (a) and photoluminescence spectra (b) of six PPVOs in chloroform solution. Both spectra show end group-dependent optical properties that are attributed to the molecular dipole and formation of aggregates states in PPVO solutions.

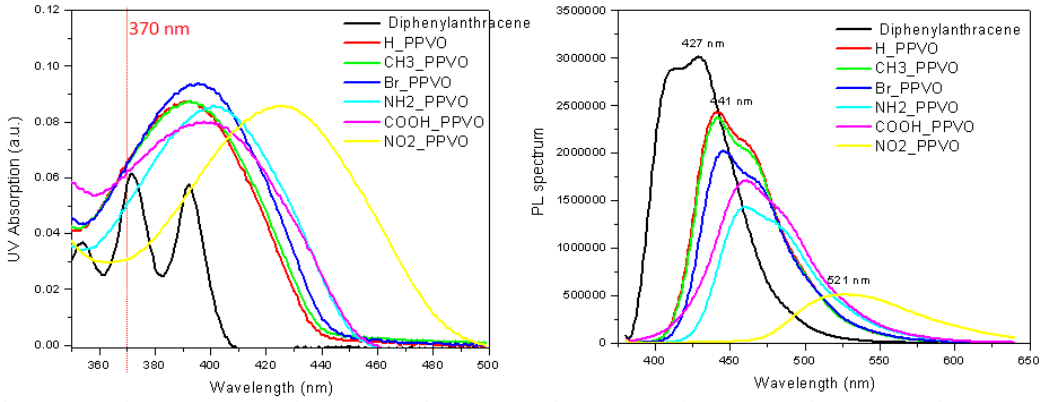

	Diphenylanthracene (DPA)	H_PPVO	CH3_PPVO	Br_PPVO	NH2_PPVO	COOH_PPVO	NO2_PPVO
Abs Intensity (a. u.) At 370 nm	0.057	0.065	0.064	0.065	0.050	0.062	0.0308
PL integral	195,645,714	161,628,531	156,543,965	135,693,088	105,924,515	134,099,468	51,272,925
Q. Y.	0.90	0.788	0.775	0.661	0.671	0.685	0.527

$Q.Y._{F(A)} = Q.Y._{F(ref)} \times (PL_A / UV_A) \times (UV_{ref}/PL_{ref}) \times (\eta_A / \eta_{ref})^2$

(η : refractive index, η of Ethanol : 1.3614, η of Toluene : 1.4969)

Solvent : Ethanol (DPA), Toluene (PPVO derivatives)

Figure S3, Determination of quantum yields of six PPVOs in toluene solution. PL spectra were recorded by excitation wavelength of 370 nm, which is different from Figure 1 in which excitation wavelength is the wavelength of max of absorbance spectra.

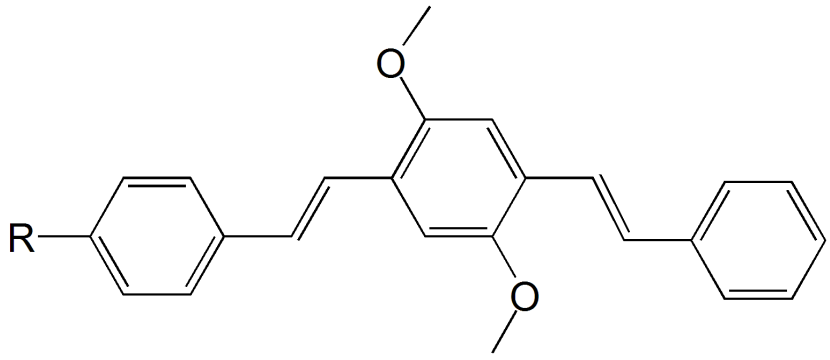

Figure S4. Alternative conformation accessible at 300K.

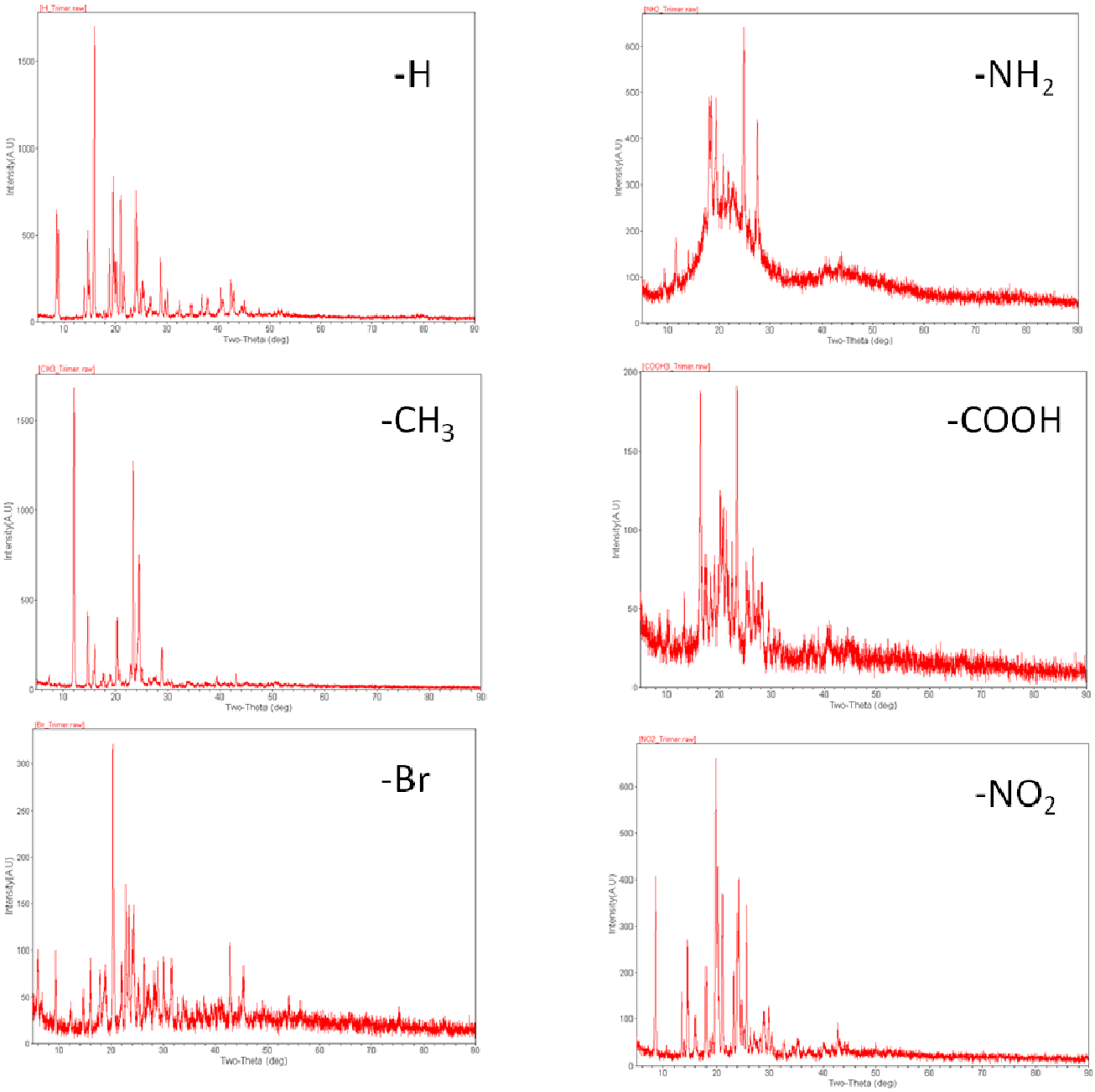

Figure S5. XRD spectra of six oligomer samples. Of all oligomer samples, we find high crystalline nature of the H-, Br- and NO2- oligomer.

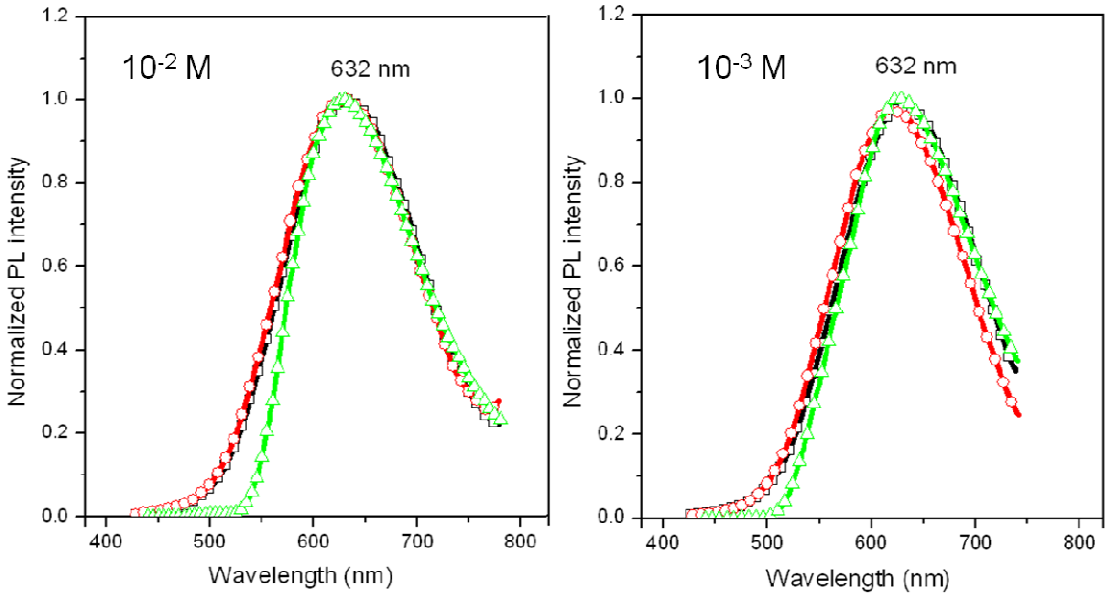

Figure S6. PL spectra of front face geometry using laser beam focus on the front of the cuvette, (—□—) and 90° angle relative to the excitation beam (—○—). PL spectrum of NO_2-OPPV in $CHCl_3$ solution (—△—) under normal PL setting.